Ptch2 loss drives myeloproliferation and myeloproliferative neoplasm progression

Claudius Klein,[1,2] Anabel Zwick,[1] Sandra Kissel,[1] Christine Ulrike Forster,[1] Dietmar Pfeifer,[1] Marie Follo,[1] Anna Lena Illert,[1] Sarah Decker,[1] Thomas Benkler,[1] Heike Pahl,[1] Robert A.J. Oostendorp,[3] Konrad Aumann,[4] Justus Duyster,[1] and Christine Dierks[1]

[1]Department of Hematology/Oncology, University Medical Center Freiburg, D-79106 Freiburg, Germany
[2]Institute for Molecular Medicine and Cell Research, University of Freiburg, D-79104 Freiburg, Germany
[3]Klinikum rechts der Isar der Technischen Universität München, III. Medizinische Klinik, 81675 München, Germany
[4]Department of Pathology, University Medical Center Freiburg, D-79104 Freiburg, Germany

JAK2V617F$^+$ myeloproliferative neoplasms (MPNs) frequently progress into leukemias, but the factors driving this process are not understood. Here, we find excess Hedgehog (HH) ligand secretion and loss of PTCH2 in myeloproliferative disease, which drives canonical and noncanonical HH-signaling. Interestingly, Ptch2$^{-/-}$ mice mimic dual pathway activation and develop a MPN-phenotype with leukocytosis (neutrophils and monocytes), strong progenitor and LKS mobilization, splenomegaly, anemia, and loss of lymphoid lineages. HSCs exhibit increased cell cycling with improved stress hematopoiesis after 5-FU treatment, and this results in HSC exhaustion over time. Cytopenias, LKS loss, and mobilization are all caused by loss of Ptch2 in the niche, whereas hematopoietic loss of Ptch2 drives leukocytosis and promotes LKS maintenance and replating capacity in vitro. Ptch2$^{-/-}$ niche cells show hyperactive noncanonical HH signaling, resulting in reduced production of essential HSC regulators (Scf, Cxcl12, and Jag1) and depletion of osteoblasts. Interestingly, Ptch2 loss in either the niche or in hematopoietic cells dramatically accelerated human JAK2V617F-driven pathogenesis, causing transformation of nonlethal chronic MPNs into aggressive lethal leukemias with >30% blasts in the peripheral blood. Our findings suggest HH ligand inhibitors as possible drug candidates that act on hematopoiesis and the niche to prevent transformation of MPNs into leukemias.

The Journal of Experimental Medicine

MPNs are characterized by a long indolent chronic period of disease with increased erythrocytes (polycythemia vera), increased thrombocytes (essential thrombocytosis) or cytopenias (osteomyelofibrosis), and splenomegaly, which frequently progress into a rapidly lethal leukemia. The mechanisms driving the disease acceleration finally leading to leukemic transformation are currently not understood.

The hedgehog (HH) signaling pathway is involved in various aspects of embryonic development and in regeneration processes during adulthood. Canonical HH pathway activation occurs via binding of HH ligands to the PATCHED (PTCH) receptors PTCH1/2, which results in release of the inhibited SMOOTHENED (SMO) receptor, followed by activation of the intracellular HH signaling complex (including SUFU) and consecutive activation of the GLI transcription factors GLI1–3. In addition, HH ligand binding to the PTCH1 receptor drives the following two SMO-independent pathways: (1) ERK phosphorylation directly mediated by the C-terminal intracellular PTCH1-signaling domain, which binds to SH3-encoding domains of proteins such as GRB2 or p85β (Chang et al., 2010) and (2) retention of activated CYCLINB1 within the cytoplasm as a result of binding to the sterol sensing domain of the PTCH receptors and therefore control of the cell cycle specifically at mitosis (Barnes et al., 2001).

The exclusive activation of the SMO-dependent canonical HH signaling pathway by point mutations in *PTCH1* (inactivating), *SMO* (activating), or *SUFU* (inactivating) drives cancer development of some specific tumor entities, such as medulloblastomas (Goodrich and Scott, 1998), rhabdomyosarcomas, and basal cell carcinomas (Gorlin, 1987). However, the majority of solid cancers (Thayer et al., 2003; Watkins et al., 2003; Datta and Datta, 2006) and especially hematologic malignancies, are driven by excess ligand secretion and therefore activate both the classical SMO-mediated canonical HH signaling and PTCH1-dependent noncanonical HH signaling, thereby stimulating ERK phosphorylation. In this situation, HH ligands not only act on the malignant cells but also stimulate the surrounding tumor-promoting stromal cells or niche cells, propagating part of their effects (Dierks et al., 2007; Chan et al., 2012; Lunardi et al., 2014). In chronic lym-

Correspondence to Christine Dierks: christine.dierks@uniklinik-freiburg.de

Abbreviations used: AML, acute myeloid leukemia; CaR, CXCL12 abundant reticular; CLL, chronic lymphocytic leukemia; DHH, Desert HH; GLI1, glioma-associated oncogene 1; GMP, granulocytic-monocytic progenitor; GRB2, growth factor receptor-bound protein 2; HH, hedgehog; MEP, megakaryocyte-erythroid progenitor; MPN, myeloproliferative neoplasm; MSPC, mesenchymal stem and progenitor cell.

The Rockefeller University Press $30.00
J. Exp. Med. 2016 Vol. 213 No. 2 273–290
www.jem.org/cgi/doi/10.1084/jem.20150556

phocytic leukemia (CLL), for example, HH ligands are produced by stromal cells and act on both CLL cells and stromal cells. CLL–stroma co-cultures are highly responsive toward treatment with HH ligand–blocking antibodies, blocking both canonical and noncanonical HH signaling, but fail in treatment with pure canonical SMO inhibitors, which is a result of the untouched hyperactive, and in this context superior, ERK survival pathway downstream of PTCH1 (Decker et al., 2012). These examples pinpoint the need for models enabling the study of the influence of hyperactive SMO-dependent canonical + PTCH1-dependent noncanonical HH signaling on malignant cells and niche cells.

In general, the studies about the role of HH signaling in hematopoiesis are highly controversial because of differences in models of fetal and adult hematopoiesis, as well as differences in the activation status of SMO-dependent, canonical and PTCH1-dependent, noncanonical HH signaling (Bhardwaj et al., 2001; Dyer et al., 2001; Byrd et al., 2002; Kobune et al., 2004; Maye et al., 2004; Gering and Patient, 2005). Previous studies of hyperactive HH signaling in adult hematopoiesis were restricted to the canonical pathway by the use of mice with Ptch1 knockout or hyperactive Smo mutations. Depletion of Ptch1 causes constitutive, canonical HH signaling caused by the release of the Smo receptor, but lacks Ptch1-dependent activation of Erk. The hematological phenotype of $Ptch1^{-/-}$ mice is characterized by a reduction in B and T cells (Uhmann et al., 2007) and an increased LKS frequency (Siggins et al., 2009) caused by cell-extrinsic, niche-dependent alterations within the BM and the thymus, whereas there were no cell-intrinsic effects within hematopoietic cells. In agreement, hyperactivation or depletion of the canonical Smo receptor or Gli1 within the hematopoietic system did not alter adult hematopoiesis (Dierks et al., 2008; Gao et al., 2009; Hofmann et al., 2009), but both genes are involved in 5-FU–induced stress hematopoiesis (Perry et al., 2009; Merchant et al., 2010) and in leukemic stem cell maintenance in BCR-ABL–driven malignant hematopoiesis (Dierks et al., 2008; Zhao et al., 2009). In conclusion, the previous findings implicate that canonical HH signaling is dispensable for normal hematopoiesis, but might be involved in stress- and BCR-ABL–driven malignant hematopoiesis. Nevertheless, the effect of regular HH pathway activation on hematopoiesis, involving ligand-mediated stimulation of combined canonical and noncanonical HH signaling, was not investigated.

We aimed to find a model system that allowed us to study the dual activation of the Smo- and Ptch1-dependent pathways in either the hematopoietic system or the hematopoietic niche. In mammals, two different Ptch receptors, Ptch1 and Ptch2 (Motoyama et al., 1998), exist. These share a similar binding capacity toward HH ligands, but Ptch2 is more stable than Ptch1 because of the lack of an ubiquitin ligase-binding site in its C-terminal tail (Kawamura et al., 2008). Similar to Ptch1, the Ptch2 receptor can regulate Smo activity, and its depletion results in canonical pathway activation, resulting in Smo activation and Gli1 transcription (Holtz et al., 2013; Alfaro et al., 2014). Furthermore, the Ptch2 receptor mediates chemotaxis and transcriptional responses to HH ligands in $Ptch1^{-/-}$ cells (Alfaro et al., 2014). In contrast to the Ptch1 receptor, the Ptch2 receptor has no C-terminal intracellular signaling domain. Therefore, we hypothesized that it would not be able to activate Erk and that, in contrast, depletion of Ptch2 might even be able to direct the complete ligand toward the Ptch1 receptor, driving increased Erk phosphorylation and simulating enhanced ligand secretion.

Indeed, our experiments demonstrate that deletion of Ptch2 not only causes Smo-dependent canonical pathway activation, but also ligand-mediated hyperactivation of the Ptch1 receptor. It also induces constitutive Erk phosphorylation, both in vitro and in vivo. The hematologic phenotype of $Ptch2^{-/-}$ mice shows features of myeloproliferative diseases, including leukocytosis, splenomegaly, progenitor mobilization, and HSC loss over time. The MPN phenotype is partially driven by the hematologic $Ptch2^{-/-}$ (leukocytosis and enhanced spleen homing), but mainly by the niche $Ptch2^{-/-}$ (cytopenias, progenitor mobilization, and HSC loss). All $Ptch2^{-/-}$ niche cells (mesenchymal stem and progenitor cells [MSPCs], osteoblasts, Cxcl12 abundant reticular [CaR] cells, and endothelial cells) display dysregulation of the canonical and/or noncanonical HH signaling pathway, causing drastic alterations in HSC regulators, such as Cxcl12, stem cell factor (Scf), and thrombopoietin (Thpo). To mimic the human situation in MPN patients, the driver oncogene JAK2V617F was combined with a $Ptch2^{-/-}$, causing hyperactive canonical and noncanonical HH signaling within the niche and/or the hematopoic system, with both driving a nonlethal myeloproliferative disease into a lethal acute leukemia.

Our findings provide an important insight into the role of ligand-driven canonical and noncanonical HH signaling and of the Ptch2 receptor on normal hematopoiesis, HSCs, and niche cells, and implicate HH ligands as drivers of myeloproliferative diseases into leukemias. Furthermore, our findings strongly support the need for alternative treatment strategies for HH ligand–driven tumors, where SMO inhibitors only target the canonical pathway but lack inhibition of Ptch1-dependent alternative HH pathways.

RESULTS

Depletion of the Ptch2 receptor induces constitutive canonical and noncanonical HH activation and recapitulates pathway activation via HH ligand overproduction

In many malignancies, HH signaling is activated at the level of ligand secretion and not via point mutations within members of the canonical HH signaling pathway. In PB leukocytes of $JAK2V617F^{+}$ MPNs and in $BCR\text{-}ABL^{+}$ CML, we observed strong overexpression of *Desert HH* (*DHH*) transcript levels (but not *SHH* or *IHH*), compared with leukocytes from normal donors or patients with acute myeloid leukemia (AML; Fig. 1 a; patient information in Table S1). *DHH* overex-

pression in MPN/CML positively correlated with elevated *PTCH1* transcript levels (Spearman correlation coefficient < 0.0001; Fig. 1 b). *PTCH1* is a direct target gene of active canonical HH signaling and suggests cell-intrinsic HH pathway activation within MPN/CML cells, but not in AML blasts.

Excess HH ligand secretion was shown to activate classical canonical HH signaling (SMO-dependent GLI1 activation), and also induces ERK phosphorylation mediated by the intracellular signaling domain of the PTCH1 receptor (noncanonical HH signaling). Therefore, HH-stimulation of PTCH1-depleted cells can only activate canonical HH signaling, but lacks activation of the PTCH1-dependent noncanonical ERK pathway. In contrast to the PTCH1 receptor, the PTCH2 receptor lacks an intracellular signaling domain. We therefore hypothesized that depletion of the PTCH2 receptor might enhance ligand binding to the PTCH1 receptor and might therefore activate both SMO-dependent canonical GLI1 activation and PTCH1-dependent noncanonical ERK activation. To identify signaling differences in between the PTCH1 and PTCH2 receptors, we analyzed canonical and noncanonical pathway activation in BM stromal cultures from Ptch1$^{+/-}$ mice, Ptch2$^{+/-}$ mice, and Ptch2$^{-/-}$ mice (genotypes; Fig. 1 c). Ptch1$^{+/-}$ BM cultures showed activated canonical HH signaling as measured by elevated *Gli1* transcription (Fig. 1 d), but as expected did not show enhanced Erk activation (Fig. 1 e). In contrast, BM stromal cells from Ptch2$^{-/-}$ mice show increased canonical Hh signaling (enhanced *Gli1* transcript levels; Fig. 1 d), but also possess strongly increased Erk phosphorylation levels (Ptch1-dependent noncanonical HH signaling; Fig. 1 e). In vitro experiments confirmed these results and show that depletion of *PTCH1* by siRNA in HH ligand–producing 293T cells causes dephosphorylation of ERK, whereas depletion of *PTCH2* actually induces ERK phosphorylation (Fig. 1 f). The Erk activation caused in Ptch2$^{-/-}$ cells was strictly dependent on the presence of HH ligands and was completely abrogated by the addition of the HH ligand–blocking antibody Shh5E1 (Fig. 1 g), confirming our hypothesis that overstimulation of the Ptch1 receptor by HH ligands in cells devoid of the competitive Ptch2 receptor causes constitutive Erk phosphorylation. In concordance, overexpression of the huPTCH1 receptor but not the huPTCH2 receptor induced ERK phosphorylation in HH ligand–producing 293T cells (Fig. 1, h and i). From our experiments, we can conclude that depletion of either receptor on its own can activate *GLI1* transcription, but only the depletion of PTCH2 induces combined canonical and noncanonical HH signaling, inducing ERK phosphorylation by directing the ligand toward the PTCH1 receptor.

Interestingly, a very similar situation was observed in many MPN and CML patients. Here, we found elevated *DHH* and *PTCH1* transcript levels in nearly all patients and, additionally, we saw a loss of *PTCH2* in 70–75% of MPN/CML cases investigated (Fig. 1 j), which could further enhance the effect of the HH ligands on the malignant cells.

Besides differences in signal transduction, the expression distribution of the Ptch1 and Ptch2 receptors might also cause differences in the hematologic phenotype. Therefore, we sorted different hematopoietic cell subsets and CD45$^-$ stromal cells from the BM of C57BL/6 mice and detected the expression of *Ptch1* and *Ptch2* via qPCR. Both receptors were expressed in all cell subsets, including LT- and ST-HSCs and nonhematopoietic stromal cells, but they showed strong differences in their expression patterns. Ptch1 was most highly expressed in lymphoid cells and proliferating erythroid cells, but only at very low levels in the granulocytic/monocytic lineages. In contrast, the Ptch2 receptor exhibited the highest transcript levels (≤80-fold) in granulocytes, monocytes, and granulocytic-monocytic progenitors (GMPs), indicating that these myeloid cells are its major effector cells and can therefore be most affected by loss of Ptch2 (Fig. 1 k).

Ptch2 depletion causes an MPN phenotype with leukocytosis, splenomegaly, and mobilization of hematopoietic progenitors

To investigate the effect of hyperactive canonical and noncanonical HH signaling on hematopoietic development, we examined the hematologic phenotype of Ptch2$^{-/-}$ mice. Blood analysis at 3, 6, and 12 mo of age showed leukocytosis in Ptch2$^{-/-}$ mice (Fig. 2 a), which was mainly driven by relative and absolute (3.5-fold at 12 mo) expansion of CD11b$^+$ granulocytes and monocytes (Fig. 2, b–d). At 12 mo of age, the PB of Ptch2$^{-/-}$ mice consisted of >60% CD11b$^+$ myeloid cells, whereas control mice were <20% (Fig. 2, b and c). Besides the expansion of mature myeloid cells, we also detected a massive increase of immature myeloid progenitors (LK cells, fourfold increase) and LKS cells (sixfold increase) mobilized into the PB of Ptch2$^{-/-}$ mice (Fig. 2 e). In contrast, T cells (both CD4$^+$ and CD8$^+$) and B cells (B220$^+$) were significantly reduced (relative and total levels; Fig. 2, b and d), and the mice developed anemia and reduced thrombocyte counts (Fig. 2 a).

The hematologic phenotype within the PB could be recapitulated in other hematopoietic organs as assessed by IHC and flow cytometry (gating strategies in Figs. S1 and S2). Both neutrophils and monocytes were expanded not only in the PB but also in BM (IHC for CD11b$^+$ cells) and spleens of Ptch2$^{-/-}$ mice, where total numbers of granulocytes and monocytes were increased three- to fourfold compared with WT mice (flow cytometry; Fig. 2, f and g).

In contrast to the monocytic and granulocytic lineage, we detected a loss of all other hematopoietic lineages within the BM. Megakaryocytes (Fig. 2, h and i), as well as megakaryocytic progenitors (MegP, Lin$^-$cKit$^+$Sca1$^-$CD41$^+$CD16/32$^-$; Fig. 2 j), the erythroid proliferation pool (CD44/Ter119 staining; Fig. 2 k), erythroid progenitors (EP, Lin$^-$cKit$^+$Sca1$^-$CD41$^-$CD16/32$^-$; Fig. 2 j), and total megakaryocyte-erythroid progenitors (MEPs; Lin$^-$cKit$^+$Sca1$^-$CD34$^-$CD16/32$^-$; Fig. 2 l) were strongly reduced within the BM compartment, explaining the anemia and thrombocytopenia detected in those mice. Reduced BM hematopoiesis in Ptch2$^{-/-}$ mice was partially

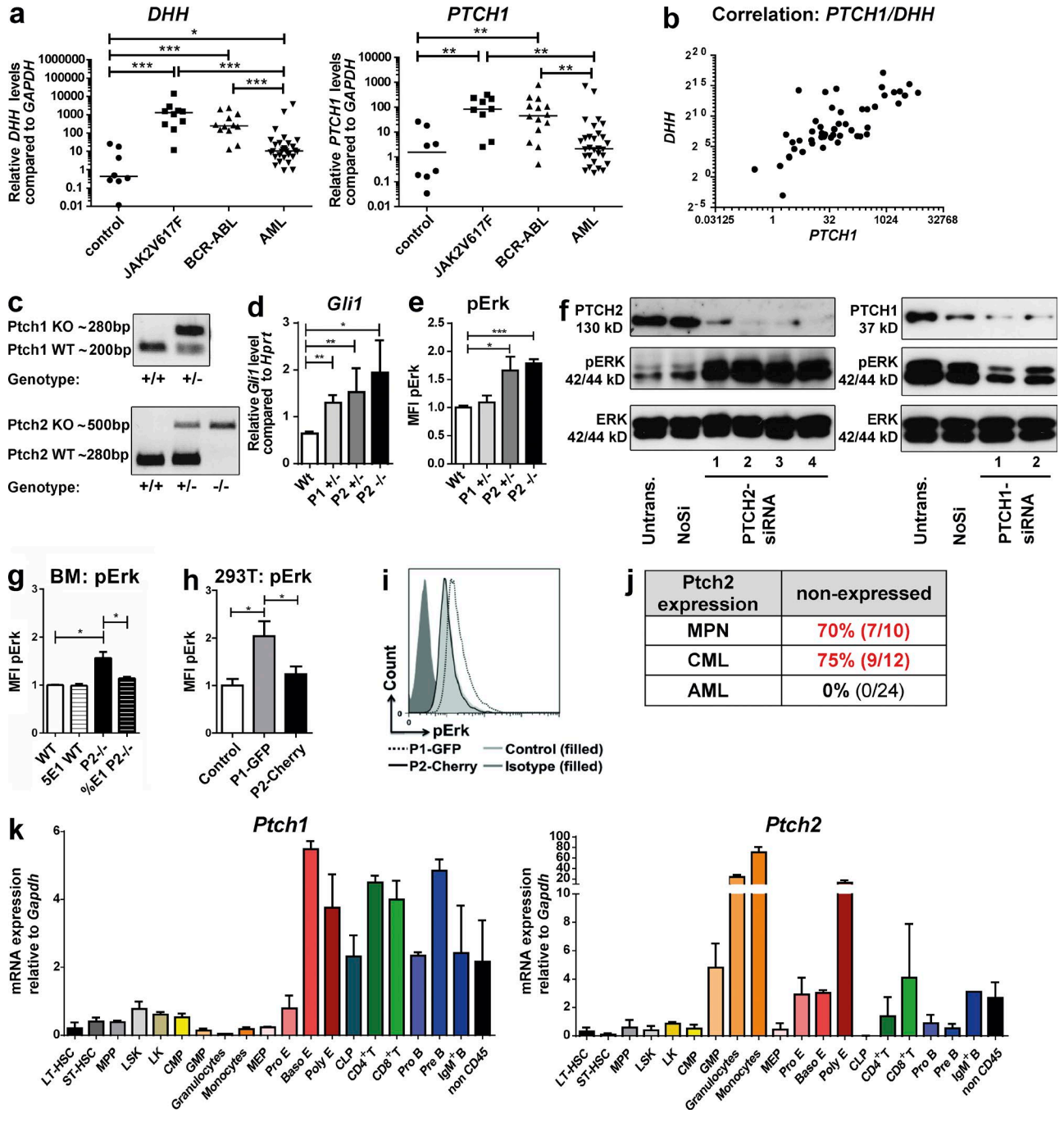

Figure 1. **Depletion of Ptch2 induces constitutive canonical and noncanonical HH activation and recapitulates pathway activation via HH ligand overproduction.** (a) qPCR for *DHH* and *PTCH1* in PB samples from patients with MPN (JAK2V617F, $n = 10$), CML (BCR-ABL, $n = 14$), or AML ($n = 29$) and controls ($n = 8$). Transcript levels are shown relative to GAPDH and compared with the median of all samples (patient single data is shown in Table S1; Mann-Whitney test). (b) Correlation between *PTCH1* and *DHH* transcript levels in the same patients as in panel a. There is a positive correlation between both genes. $P < 0.0001$, Spearman correlation coefficient; $r = 0.7351$. (c) Detection of murine *Ptch1* and *Ptch2* WT and KO allele using PCR for genotyping. (d) qPCR for *Gli1* in murine BM stroma samples (cultivated for 12 d without cytokines) from WT, Ptch1$^{+/-}$, Ptch2$^{+/-}$, and Ptch2$^{-/-}$ mice. Transcript levels are shown relative to *Hprt* and compared with the median of all samples ($n \geq 3$, unpaired Student's *t* test). (e) Intracellular pErk staining in murine BM stroma cells, normalized to WT control ($n \geq 4$, unpaired Student's *t* test). (f) Western blot of 293T cells transfected with four different *PTCH2* or two different *PTCH1* siRNAs and blotted with antibodies against PTCH1, PTCH2, pERK, and total ERK. One out of two independent experiments. (g) Intracellular pErk staining in WT ($n = 3$) versus Ptch2$^{-/-}$ ($n = 4$) BM cells treated for 24 h with 5E1 or IgG control Ab, normalized to the WT control (unpaired Student's *t* test). (h and i) pERK measurement in 293T cells transfected with *GFP-Ctrl* ($n = 5$), *PTCH1-GFP* ($n = 4$), or *PTCH2-Cherry* ($n = 5$), normalized to *GFP-Ctrl* (unpaired Student's *t* test). A representative example is shown in panel i. (j) qPCR for *PTCH2* in PB samples from patients with MPN (JAK2V617F^{+}, $n = 10$), CML (BCR-

compensated for by enhanced extramedullary hematopoiesis with increased spleen weight and increased spleen cellularity (Fig. 2, m–o). Cells delocalized into the spleen were immature LKS cells, LK cells consisting mainly of MEPs and GMPs (Fig. 2 l) and mature myeloid cells ($Ter119^+$ erythroid cells, granulocytes, and monocytes, Fig. 2, f and k). FACS data could be confirmed by colony assays showing a strong increase of erythroid colonies (CFU-Es) and granulocyte/monocyte colonies (CFU-GMs) within the spleen (Fig. 2 p). Similar to MPN patients, immature myeloid cells and colony forming cells (CFU-GMs and CFU-Es) were strongly increased in the PB of $Ptch2^{-/-}$ mice (Fig. 2 p).

In conclusion, the $Ptch2^{-/-}$ hematopoietic phenotype shows many features of human MPN patients with expansion of the granulocyte/monocyte compartment, enhanced extramedullary hematopoiesis with splenomegaly, and increased progenitor/LKS mobilization into the peripheral blood.

$Ptch2^{-/-}$ causes a progressive loss of B and T lymphocytes

In contrast to granulocytes and monocytes, both lymphoid cell populations were progressively lost in $Ptch2^{-/-}$ mice. T cells were consistently reduced in the PB, the spleen (involving both $CD4^+$ and $CD8^+$ T cells) and in the developing thymus of 3-mo-old mice and at all later time points (Fig. 3, a and b). Reduced thymocytes (46×10^6 [WT] to 32×10^6 [KO]) involved all major thymic T cell subpopulations including $CD4^-CD8^-$, $CD4^+CD8^+$, and both single-positive cell types, whereas relation in between the different T cell subsets was not altered (Fig. 3, c and d). All T cell subsets within the thymus showed a significant and strong increase in spontaneous apoptosis rates, pointing toward alterations within the selection process caused by depletion of Ptch2 (Fig. 3, b, e, and f).

B cells were normal at 3 mo, but strongly reduced in the PB, the BM, and the spleen at 12 mo (Fig. 2, b-d and Fig. 3, g and h). Impairment of B cell development already started at the earliest step of B/T cell–specific development, the CLP population (Fig. 3 g). Most additional steps of B cell development within the BM (pro–B cells, pre–B cells, and immature B cells) and the spleen (T1, T2, and T3 B cells) were reduced, pointing toward the lack of early progenitors being causative for reduction of B cell progenitors starting at the CLP stage and an additional loss at the transition from prepro–B cells to pro–B cells (Fig. 3 g).

$Ptch2^{-/-}$ causes increased HSC cell cycling, leading to HSC exhaustion, but improves resistance to 5-FU–induced stress hematopoiesis

We further examined the effect of $Ptch2^{-/-}$ on the HSC compartment. Gating strategies are described in Figs. S1 and S2. At 3 mo of age, we found a relative and total increase in LKS cells within the BM and within spleens of $Ptch2^{-/-}$ mice (Fig. 4 a). Cell cycle analysis using EDU click assay and FxCycle violet stain revealed increased cells in S/G2/M phase within all LKS subsets (MPPs, ST-HSCs, LT-HSCs) and also within the myeloid progenitor compartment (Fig. 4, b and c), explaining the drive toward increased myelopoiesis and leukocytosis seen in those mice. In addition, $Ptch2^{-/-}$ mice show a reduction of quiescent HSCs in G_0 (Ki67/FxCycle violet stain; Fig. 4 d). These cell cycle changes resulted in a significant loss and exhaustion of HSCs over time, resulting in a reduction of LT-HSCs by 50% at 12 mo of age as assessed by flow cytometry using three different staining strategies of LKS cell subpopulations (Fig. 4, a, e, and f; and Fig. S1). Not only were LT-HSCs reduced, but so were all subsequent differentiation steps, such as ST-HSCs and MPPs (Fig. 4 f). Loss of repopulating LT-HSCs was also confirmed by performing a limiting dilution assay that showed a reduced CRU frequency of 1:33.361 in $Ptch2^{-/-}$ mice versus 1:17.246 in WT mice (Fig. 4, g and h).

To directly compare the functionality of LT-HSCs from $Ptch2^{-/-}$ mice versus WT mice, we performed a HSC competition assay and sorted 150 LT-HSCs ($Lin^-Kit^+Sca^+CD150^+CD48^-$) from $Ptch2^{-/-}$ versus WT BM (both $CD45.2^+$) and diluted them with 1×10^6 supporter BM cells ($CD45.1^+$) and transplanted those into mixed CD45.1/CD45.2-expressing mice (Fig. 4, g and i). Chimerism in the PB was first assessed at 3 wk after transplantation and showed a slightly enhanced early engraftment for the faster cycling $Ptch2^{-/-}$ LT-HSCs, which turned into a reduced, but stable long-term engraftment after 6–14 wk, suggesting a functional defect of the $Ptch2^{-/-}$ LT-HSCs (Fig. 4 i). Interestingly, the frequency of $Ptch2^{-/-}$ $CD45.2^+$ cells did not decrease further, but slightly increased over time, giving us the first evidence that $Ptch2^{-/-}$ HSCs in a normal WT niche do not suffer losses, and might even regain self-renewal properties.

Enhanced cell cycle within LT-HSCs increases the probability of differentiation and can cause exhaustion of the LT-HSC pool over time, but can be of advantage regarding stress hematopoiesis induced by low-dose 5-FU (150 mg/kg bw; Campaner et al., 2013). We therefore challenged the regeneration capacity of 3-mo-old mice by injecting them with 5-FU, which induces apoptosis in actively cycling cells and causes severe aplasia. As expected, 5-FU treatment more efficiently depleted the BM, reduced hemoglobin levels, and decreased WBC counts in the more actively cycling $Ptch2^{-/-}$ mice compared with WT mice, 5 d after 5-FU injection (Fig. 4 j). At 7 d after 5-FU treatment, WBCs and hemoglobin levels were equivalently reduced in both groups (Fig. 4j). But in contrast to the previous measurement, total BM cells were already increased in $Ptch2^{-/-}$ mice compared with WT mice,

ABL, $n = 12$), or AML ($n = 24$; patient single data is shown in Table S1). (k) qPCR for *Ptch1* and *Ptch2* in different BM cell subsets ($n = 3$–5 per cell subset, sorting/gating strategies are shown in Fig. S1). Transcript levels are shown relative to Gapdh and compared with the median of all samples. *, $P < 0.05$; **, $P < 0.01$; ***, $P < 0.001$.

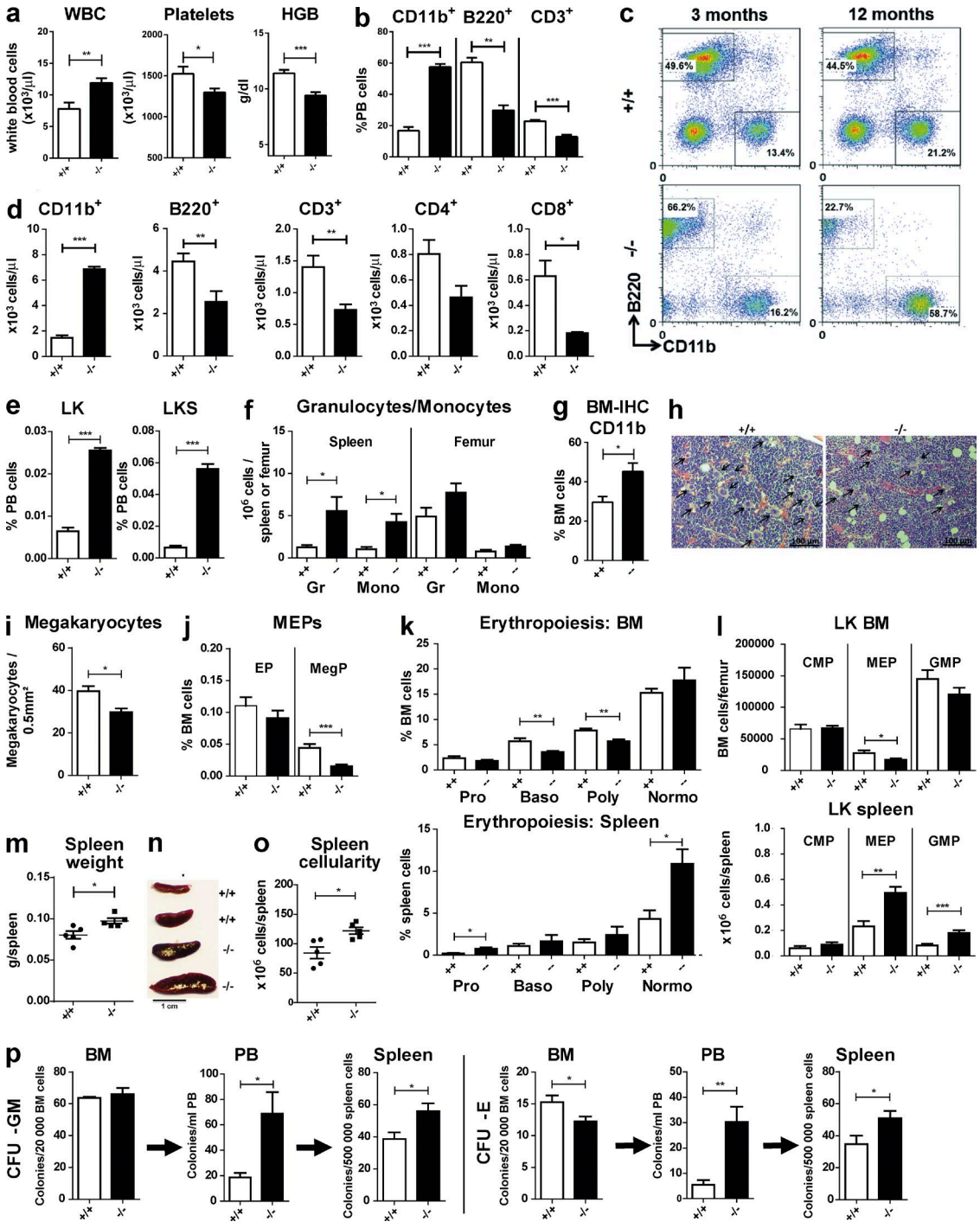

Figure 2. **Ptch2 depletion causes an MPN phenotype with leukocytosis, splenomegaly, and mobilization of hematopoietic progenitors.** (a) PB samples were analyzed for WBC counts, platelets, and hemoglobin (HGB) at 12 mo of age using the Scil Animal Blood Counter ($n \geq 9$ each genotype, unpaired Student's *t* test was performed for statistics throughout this figure). (b) Flow cytometry analysis for $CD11b^+$ (myeloid cells), $B220^+$ (B cells), and $CD3^+CD90^+$ (T cells) in the PB at12 mo of age ($n \geq 5$ each genotype). (c) Flow cytometry analysis of PB cells of WT and $Ptch2^{-/-}$ mice after 3 and 12 mo. CD11b/B220 staining of a representative example is shown for each time point and genotype. $B220^+$ cells represents the B cell population, $CD11b^+$ cells represents granulocytes and monocytes. (d) Total $CD11b^+$ (myeloid cells), $B220^+$ (B cells), and $CD3^+CD90^+$ (T cells, subdivided into $CD4^+$ and $CD8^+$) in the PB ($n \geq 3$ each genotype, 12 mo). (e) Ficolized PB was analyzed for LK ($Lin^-cKit^+Sca1^-$) and LKS ($Lin^-cKit^+Sca1^+$) cells using flow cytometry ($n \geq 3$ each genotype). (f) Total granulocytes ($CD11b^+Ly6G^+$) and monocytes ($CD11b^+Ly6G^-$) within the spleen and femur ($n \geq 5$ each genotype, 12 mo). (g) Percentage of $CD11b^+$ cells within the BM of WT versus $Ptch2^{-/-}$ mice. Cells were quantified after IHC staining with a $CD11b^+$ antibody using the high content screen scanR ($n = 5$ each genotype, 3 mo). (h) Representative images from hematoxylin and eosin (H&E)–stained BM slides of WT and $Ptch2^{-/-}$mice. Arrowheads

indicating faster BM regeneration in those mice (Fig. 4 j, bottom). Furthermore, LSK^{med} cells, representing the regenerating and proliferating LKS population (Campaner et al., 2013), were strongly increased in the regenerating Ptch2$^{-/-}$ BM compared with WT BM, resulting in increased myeloid progenitors and also a faster increase in LKS cells (Fig. 4, k and l). Cell cycle analysis revealed that, even during BM regeneration, the cell cycle was increased in Ptch2$^{-/-}$ mice compared with WT mice (Fig. 4, m and n). The accelerated regeneration capacity of Ptch2$^{-/-}$ mice also translated into a significantly better survival after weekly 5-FU injections (Fig. 4 o), supporting the advantage of hyperactive canonical and noncanonical HH signaling for 5-FU–induced stress hematopoiesis.

In conclusion, the increased cell cycle and reduced quiescence of HSCs in Ptch2$^{-/-}$ mice results in a reduction of HSCs over time, but enhances the regeneration capacity of the bone marrow after 5-FU–induced aplasia in young mice.

Niche change experiments reveal counteracting functions of cell-intrinsic and -extrinsic ligand-driven HH signaling on hematopoiesis

We next evaluated whether the observed phenotype in Ptch2$^{-/-}$ mice is a result of hyperactive canonical and noncanonical HH signaling in the niche or within the hematopoietic system. Therefore, we performed the niche change transplantation system shown in Fig. 5 a: black, control (CD45.2$^+$ WT BM was transplanted into CD45.1$^+$ WT mice); blue, hematopoietic Ptch2$^{-/-}$ (CD45.2$^+$ Ptch2$^{-/-}$ BM was transplanted into CD45.1$^+$ WT mice); red, niche Ptch2$^{-/-}$ (CD45.1$^+$ WT BM was transplanted into CD45.2$^+$ Ptch2$^{-/-}$ mice). Chimerism was between 97 and 100% 3 mo after transplantation (unpublished data). Ptch2$^{-/-}$ mice with WT BM (red) developed a pancytopenia with reduced leukocytes, mainly caused by decreased B and T cells, reduced thrombocyte counts, and reduced hemoglobin levels (Fig. 5, b and c), whereas granulocyte/monocyte levels were normal. BM analysis revealed that the Ptch2$^{-/-}$ niche caused reduction of megakaryocytes, erythroid progenitors, MEPs, colony forming cells, LK cells, and LKS cells (Fig. 5, d–h). Within the HSC compartment, all HSC subsets were reduced, including LT-HSCs (Fig. 5 h). Loss of LT-HSCs could be confirmed via a limiting dilution assay of BM cells from mice 4 mo after the first niche change experiment, demonstrating a strongly reduced CRU frequency of 1:90.091 in mice with the Ptch2$^{-/-}$ niche compared with 1:26.909 in the control group (Fig. 5 i). Long-term follow-up of mice with WT BM in a Ptch2$^{-/-}$ niche (red) showed a shortened survival as a result of increasing cytopenias caused by the reduced regeneration pool (Fig. 5 j). Also, the reduction of thymic cells and the increased apoptosis rates within the thymic T cell subpopulations was dependent on the cell-extrinsic Ptch2$^{-/-}$ (Fig. 5 k). Furthermore, loss of B cells starting at the CLP level was dependent on the niche Ptch2$^{-/-}$ (unpublished data). In addition, we found that the mobilization of colony-forming cells, including progenitor and LKS cells, into the PB was also dependent on the cell-extrinsic hyperactivation of HH signaling in the niche (Fig. 5 l).

In contrast, the hematologic Ptch2$^{-/-}$ phenotype (Ptch2$^{-/-}$ BM in a WT mouse, blue) was characterized by leukocytosis resulting from an expansion of all cell subsets, including granulocytes, T cells, and B cells (Fig. 5, b and c). Hemoglobin levels and thrombocytes increased to normal levels within 4 mo after transplantation. Ptch2$^{-/-}$ BM in a WT niche had no defect in LKS frequency and function (Fig. 5, h–j). In contrast, the in vitro replating of either 1% or of total cell numbers of 1,000 or 5,000 cells showed that the hematopoietic Ptch2$^{-/-}$ significantly increased replating capacity at replating rounds 3–5 (Fig. 5, m and n). Further evaluation of the replated cells by flow cytometry showed that the Ptch2$^{-/-}$ significantly enhanced the frequency of LKS cells from replating round to replating round (Fig. 5 o). In addition, homing experiments showed that all transplantation groups had similar homing capacities into the BM, but that the hematopoietic Ptch2$^{-/-}$ increased the homing of hematopoietic cells into the spleen (Fig. 5 p).

Table 1 summarizes the findings from the niche change experiment. We can conclude that hyperactivation of canonical and noncanonical HH signaling in the niche causes depletion of hematopoiesis starting with the LT-HSC compartment, causes progenitor mobilization, and also affects selection processes in the thymus and B cell lymphopoiesis. In contrast, the cell-intrinsic hyperactivation of canonical and noncanonical HH signaling causes leukocytosis and can enhance self-renewal properties, as well as homing into the spleen.

The Ptch2$^{-/-}$ causes depletion of osteoblasts and alters expression of essential HSC retention and maintenance factors within all niche cell subsets

Because the major hematopoietic changes apparent in our mice, particularly the loss of LT-HSCs and the mobilization of progenitors into the PB, are caused by cell-extrinsic effects,

indicate megakaryocytes (3 mo). Bars, 100 µm. (i) Megakaryocyte count per 0.5 mm^2 as assessed on H&E-stained BM slides ($n \geq 4$ per genotype). (j) Flow cytometry analysis of megakaryocytic progenitors (MegP, Lin$^-$cKit$^+$Sca1$^-$CD41$^+$CD16/32^{low}, $n = 10$ each genotype, 3 mo) and erythroid progenitors (EP, Lin$^-$cKit$^+$Sca1$^-$CD41$^-$CD16/32$^-$). (k) BM and spleen erythropoiesis ($n \geq 4$ each genotype, 12 mo). Proerythroblasts (Pro), basophilic eryhtroblasts (Baso), polychromatic erythroblasts (Poly), normoblasts, and reticulocytes (Retic). (l) Flow cytometry analysis of BM and spleen LK (Lin$^-$cKit$^+$Sca1$^-$) cells subdivided into CMPs (Lin$^-$cKit$^+$Sca1$^-$CD34$^+$CD16/32^{mid}), MEPs (Lin$^-$cKit$^+$Sca1$^-$CD34$^-$CD16/32$^-$), and GMPs (Lin$^-$cKit$^+$Sca1$^-$CD34$^+$CD16/32$^+$; $n \geq 10$ each genotype, 3 mo). MEPs and GMPs are reduced in the BM, but increased in the spleen of Ptch2$^{-/-}$ mice. (m) Spleen weight shown as single values and as the mean of all samples within WT and Ptch2$^{-/-}$ mice ($n = 5$ each genotype, 3 mo). (n) Representative image of WT and Ptch2$^{-/-}$ spleens. (o) Spleen cell counts ($n = 5$ each genotype, 3 mo). (p) Colony assay performed with 2×10^4 BM cells, 5×10^5 PB cells, and 2×10^5 spleen cells in MethoCult3434. The numbers of CFU-GM and CFU-E were counted after 7 d ($n = 4$ each genotype performed in duplicates, 3 mo). *, $P < 0.05$; **, $P < 0.01$; ***, $P < 0.001$.

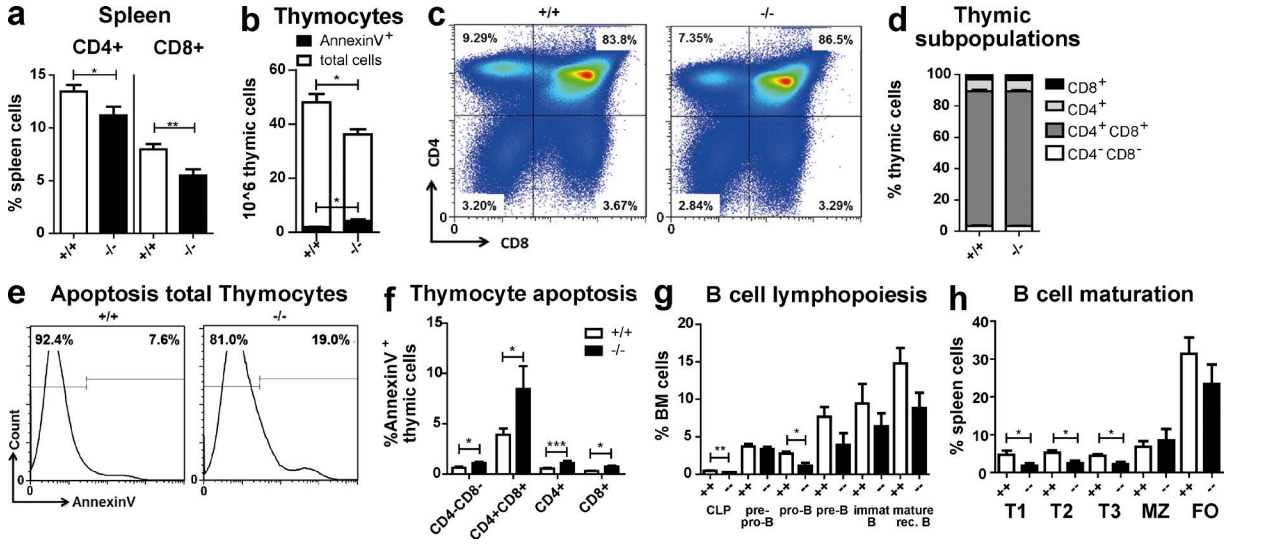

Figure 3. **Ptch2$^{-/-}$ causes a progressive loss of B and T lymphocytes.** (a) CD3$^+$CD90$^+$CD4$^+$ and CD3$^+$CD90$^+$CD8$^+$ cells in the spleen of WT and Ptch2$^{-/-}$ mice (pooled data of two independent experiments, $n \geq 9$ each genotype, 3 mo, unpaired Student's *t* test). (b) Total (open bars) and total apoptotic (filled bar, Annexin V$^+$) thymocytes in WT versus Ptch2$^{-/-}$ mice ($n = 5$ each genotype, 3 mo, two independent experiments, unpaired Student's *t* test). (c) Flow cytometry analysis of thymocytes (WT versus Ptch2$^{-/-}$ mice) after 3 mo. CD4/CD8 staining of a representative example is shown for each genotype. (d) Distribution of thymic subpopulations (CD4$^+$, CD8$^+$, CD4$^+$CD8$^+$, and CD4$^-$CD8$^-$; $n \geq 5$ each genotype, 3 mo, two independent experiments, unpaired Student's *t* test). (e) Flow cytometry analysis of total thymocytes (WT versus Ptch2$^{-/-}$ mice) after 3 mo. Annexin V staining of a representative example is shown for each genotype. (f) Thymic subpopulations CD4$^+$, CD8$^+$, CD4$^+$CD8$^+$, and CD4$^-$CD8$^-$ were analyzed for apoptosis (Annexin V$^+$) levels ($n \geq 5$ each genotype, 3 mo, two independent experiments, unpaired Student's *t* test). (g) Flow cytometry analysis for B cell lymphopoiesis within the BM of WT and Ptch2$^{-/-}$ mice after 12 mo. B220$^+$ BM cells were subdivided into mature (B220$^+$IgM$^{+/-}$IgD$^+$), immature (B220$^+$IgM$^+$IgD$^-$), prepro–B cells (B220$^+$IgM$^-$IgD$^-$CD43$^+$CD24$^-$), pro–B cells (B220$^+$IgM$^-$IgD$^-$CD43$^+$CD24$^+$), and pre–B cells (B220$^+$IgM$^-$IgD$^-$CD43$^-$CD24$^+$). Also CLPs (Lin$^{-(-Il7R)}$ cKit^{med} Sca1^{med} Flt3$^+$ Il7R$^+$) are shown ($n \geq 3$ each genotype, two independent experiments, unpaired Student's *t* test). (h) Flow cytometry analysis for B cell maturation within the spleen of WT and Ptch2$^{-/-}$ mice after 12 mo. Mature B cells were subdivided into marginal zone (MZ) B cells (CD19$^+$CD93$^-$CD23$^-$IgM$^+$) and follicular (FO) B cells (CD19$^+$CD93$^-$CD23$^+$IgM$^{-/+}$). Immature B cells were subdivided into transitional (T) B cells T1 (CD19$^+$CD93$^+$CD23$^-$IgM$^+$), T2 (CD19$^+$CD93$^+$CD23$^+$IgM$^+$), and T3 (CD19$^+$CD93$^+$CD23$^+$IgM$^-$) cells ($n \geq 3$ each genotype, two independent experiments, unpaired Student's *t* test). *, $P < 0.05$; **, $P < 0.01$; ***, $P < 0.001$.

we aimed to identify alterations of the hematopoietic niche in Ptch2$^{-/-}$ mice. The BM niche consists of various cell types, such as osteoblasts, endothelial cells, CaR cells, and MSPCs. These provide factors essential for stem cell maintenance, stem cell differentiation, homing, and retention in the BM. Bone sections revealed a decreased frequency of endosteal osteoblasts and slightly reduced bone substance in Ptch2$^{-/-}$ mice (Fig. 6, a and b). Furthermore, in vitro BM stromal cultures from Ptch2$^{-/-}$ versus WT BM for 12 d showed reduced expression of several important HSC regulators (Fig. 6 c): Cxcl12, which regulates HSC retention in the BM and HSC quiescence, as well as multilineage reconstitution (Sugiyama et al., 2006; Greenbaum et al., 2013); Jagged1 (Jag1), which was shown to be required for quiescence and self-renewal of HSCs (Poulos et al., 2013; Mendelson and Frenette, 2014); and angiopoietin-1. Next, we sorted osteoblasts, CaR cells, endosteal cells, and MSPCs fromBM and from digested bones of Ptch2$^{-/-}$ versus WT mice (gating strategy in Fig. S1). RNA from sorted niche cells was amplified, and we performed qPCR for *Smo*, *Ptch1*, *Ptch2*,*Dhh*, and for HSC regulators, in addition to microarray gene expression analysis. *Smo* was preferentially expressed in MSPCs and osteoblasts, indicating that these niche cell subsets are the most sensitive to alterations within the canonical HH signaling pathway (Fig. 6 d). In agreement with this, the canonical HH signaling pathway (represented in the KEGG pathway analysis as HH and basal cell carcinoma pathway) was only activated in MSPCs, but not in other niche cells (Fig. 6 e and Fig. S3). *Ptch1* and *Ptch2* were expressed in all niche cells, with *Ptch1* being most highly expressed in endothelial cells and *Ptch2* in MSPCs. Interestingly, the Ptch1 receptor-dependent noncanonical Erk pathway represented as Ras signature pathway (oncogenic signature and Kegg gene sets in Fig. S3 and Table S2) was activated in all four niche cell subsets, indicating that noncanonical HH signaling is considerably more involved than the canonical pathway. *Dhh* was exclusively expressed in endothelial cells, pointing to these cells as being the natural regulators of HH signaling within the niche (Fig. 6 d). qPCR for essential HSC regulators shows that all niche cells are involved in deregulation of niche homeostasis in Ptch2$^{-/-}$ mice and confirms the data from the BM stromal cultures (Fig. 6, c and f). *Scf* is down-regulated in all Scf-expressing niche cells, especially endothelial cells and CaR cells. *Cxcl12*, the major retention factor in the niche, is down-regulated in CaR cells, but also in osteoblasts. *Osteopontin* is most highly expressed and strongly down-regulated in osteoblasts. *Angiopoietin-1*

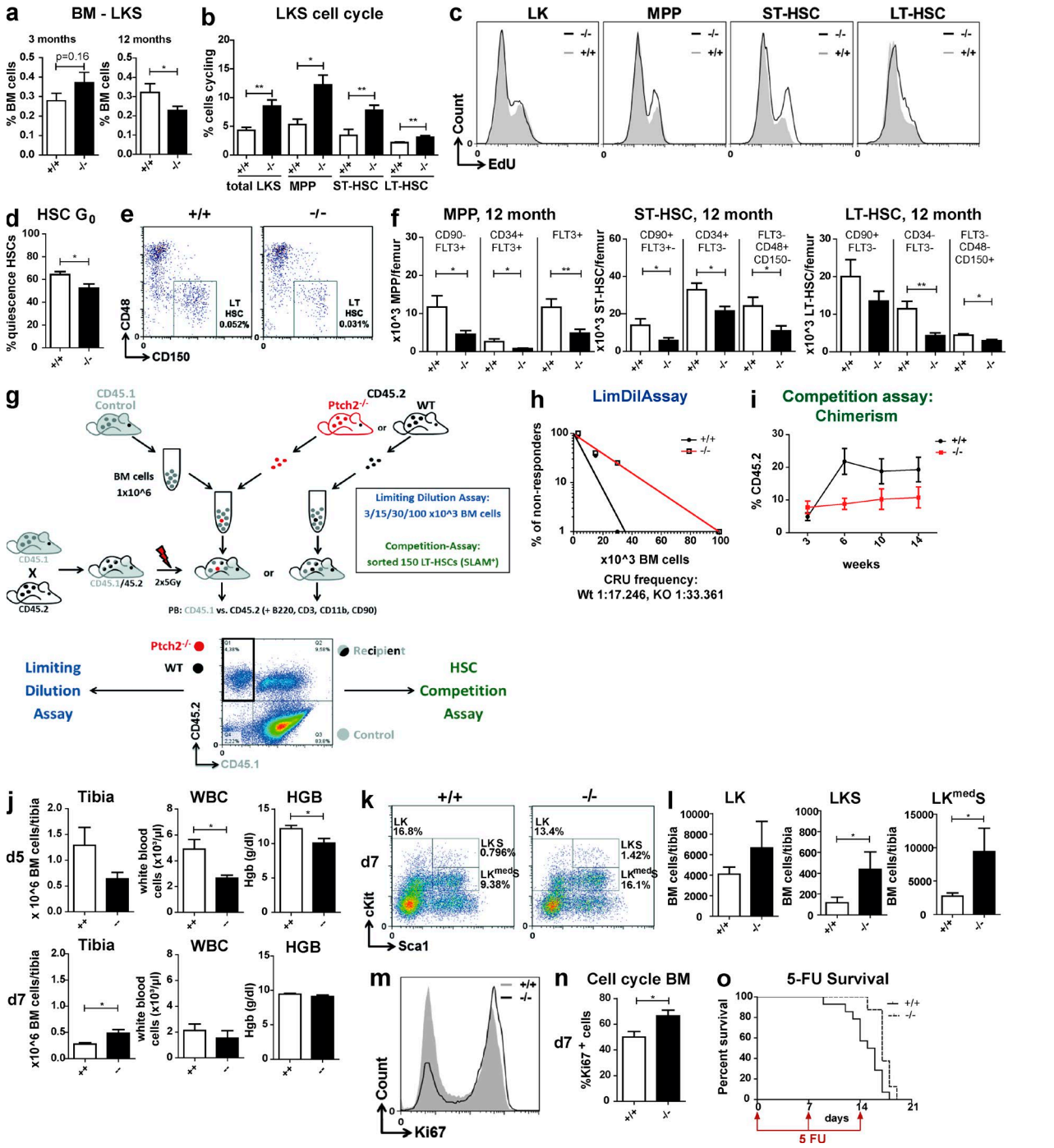

Figure 4. **Ptch2$^{-/-}$ causes increased HSC cell cycling, leading to HSC exhaustion, but improves resistance to 5-FU–induced stress hematopoiesis.** (a) Total LKS ($Lin^-cKit^+Sca1^+$) cells within the BM as assessed by flow cytometry analysis ($n \geq 6$ each genotype) at 3 and 12 mo of age (two independent experiments, unpaired Student's *t* test). (b) Total LT-HSCs ($Lin^-cKit^+Sca1^+FLT3^-CD48^-CD150^+$), ST-HSCs ($Lin^-cKit^+Sca1^+FLT3^-CD48^+CD150^-$), MPPs ($Lin^-cKit^+Sca1^+FLT3^+$), and total HSCs. Cell cycle was measured using FxCycle Violet Stain ($n = 3$, two independent experiments, unpaired Student's *t* test). (c) Cell proliferation of myeloid progenitors (LK cells) and HSC subpopulations of WT versus Ptch2$^{-/-}$ mice after 15 h of i.p. EdU injection and sorting of HSC subpopulations (BM of five mice was pooled for each genotype). (d) HSC cell cycle analysis of WT and Ptch2$^{-/-}$ BM cells using Ki67 and FxCycle Violet. Graph demonstrates the percentage of quiescent cells ($n = 4$ each group, unpaired Student's *t* test, staining is illustrated in Fig. S2). (e) Representative dot plots of LT-HSCs ($Lin^-cKit^+Sca1^+FLT3^-CD150^+CD48^-$) are shown for each genotype (12 mo). (f) HSC subpopulations in WT versus Ptch2$^{-/-}$ mice measured by three different HSC stainings: ($Lin^-cKit^+Sca1^+$ plus FLT3/CD90 or plus CD34/FLT3 or plus FLT3/CD48/CD150, gating strategies: Fig. S1, $n \geq 6$ each genotype, 12 mo, two independent experiments, unpaired Student's *t* test). (g) Transplantation scheme for limiting dilution and competition HSC assays. For LimDilAssays

is reduced in CaR cells and osteoblasts, but maintained at high levels in MSPCs. *Jagged1* is down-regulated in endothelial cells, where it is normally highly expressed. Interestingly, *thrombopoietin* (*Thpo*), a strong regulator of HSC quiescence and proliferation, is strongly up-regulated in osteoblasts and MSPCs. Although low levels of Thpo restrain HSCs in a quiescent state, high Thpo levels drive HSC proliferation and could therefore result in the increase in cell cycling detected in the HSC compartment of Ptch2$^{-/-}$ mice.

From these experiments, we can conclude that the niche is strongly affected by alterations in canonical, and even more by the noncanonical, HH signaling pathway, and that essential factors for stem cell maintenance, such as Scf and Jagged1, stem cell proliferation as in Thpo, or retention factors such as Cxcl12 are all strongly affected and could be involved in reduced HSC numbers and enhanced HSC mobilization seen in Ptch2$^{-/-}$ mice.

The cell-intrinsic, but also –extrinsic, Ptch2$^{-/-}$ accelerates myeloproliferative diseases caused by JAK2V617F and converts a chronic polycythemia vera–like disease into a lethal leukemia

Our initial experiments show that the majority of patients with chronic myeloproliferative diseases have an overexpression of DHH ligands within hematopoietic cells, which may autostimulate hematopoietic cells or stimulate HH-responsive niche cells. To distinguish the influence of niche-dependent HH activation versus cell-intrinsic HH activation on disease development, we performed the niche change experiment again, but in this experiment we infected the BM cells with retroviral particles containing either the BCR-ABL/GFP oncogene or the JAK2V617F/GFP oncogene.

The expression of the JAK2V617F oncogene in C57BL/6 mice causes a myeloproliferative disease characterized by increased hemoglobin/hematocrit in the initial phase of the disease, followed by leukocytosis (granulocytes/monocytes) in the PB. In addition, the mice develop increased extramedullary hematopoiesis with splenomegaly and low-grade myelofibrosis, but they do not die from this chronic disease. Interestingly, the hyperactivation of canonical and noncanonical HH signaling either within the niche or within the hematopoietic system or both drastically enhanced the JAK2V617F disease phenotype and turned the chronic myeloproliferative disease into a lethal leukemic disease (Fig. 7 a). The combination of JAK2V617F and the hematopoietic Ptch2$^{-/-}$ caused a massively increased leukocytosis in the PB consisting of mature CD11b^{+} myeloid cells (Fig. 7 b) and also CD11b^{+}Kit^{+} immature blasts accounting for 15% of total PB leukocytes (Fig. 7 b). Immature cells were also increased in BM and spleens, and the accelerated disease resulted in the death of 6/10 mice. JAK2V617F plus the Ptch2$^{-/-}$ niche did not enhance leukocytosis or splenomegaly. In contrast, the mice developed a more severe thrombocytopenia and anemia (HGB < 6 g/dl). Furthermore, they showed an increased mobilization of cKit^{+} cells into the PB, accounting for 20% of leukocytes and fulfilling the criteria for an acute myeloid leukemia (Fig. 7 b). Combined depletion of Ptch2 in the niche and the BM showed the most severe phenotype, and all of the mice died from the JAK2V617F-driven disease within 1 yr of transplantation (Fig. 7 a). At the 3-mo time point, the majority of mice had >25% blasts in the PB, had developed thrombocytopenia (Fig. 7 b), and had developed a significantly increased splenomegaly (Fig. 7, d and e). BM aspiration 100 d after treatment showed that the polycythemia vera phenotype with massively increased Ter119^{+} erythroid progenitors had already turned into a granulopoiesis-driven phenotype with increased Gr-1^{+}/CD11b^{+} cells and increased cKit^{+} immature progenitors within the BM and the PB in Ptch2$^{-/-}$ mice (Fig. 7 c). Investigation of JAK2V617F^{+} LKS and LK cells at the time of death revealed that the addition of Ptch2 within hematopoiesis and the niche favors the expansion of the immature malignant cells primarily in the spleen, but also in the BM, creating a leukemia-promoting environment (Fig. 7 f). Despite the presence of the JAK2V617F oncogene, we found similar alterations in cytokines expressed by the Ptch2$^{-/-}$ niche cells, especially down-regulation of *Cxcl12* and *Scf* (Fig. 7 g).

In contrast to JAK2V617F, the BCR-ABL oncogene always causes a lethal myeloproliferative disease in C57BL/6

3, 15, 30, or 100 × 10^{3} BM cells from WT mice (12 mo, CD45.2, WT [black], or Ptch2$^{-/-}$ mice [red]) were pooled with 10^{6} supporting BM cells (CD45.1, gray) and transplanted into lethally irradiated CD45.1/45.2 expressing mice (n > 6 per group). For competition LT-HSC assays, 150 sorted LT-HSCs from WT versus Ptch2$^{-/-}$ BM cells (12 mo, both CD45.2^{+}) were each pooled with 10^{6} competitor control BM cells (CD45.1^{+}) and transplanted into irradiated CD45.1/45.2-expressing mice (n > 9 per genotype). Representative PB dot plot 3 wk after treatment is shown. CD45.1 single-positive cells represent the PB cells generated by the control/competitor BM. CD45.1/CD45.2 double pos. cells represent the remaining blood cells of the recipient mouse. CD45.2^{+} cells represent our cells of interest generated from total BM (limiting dilution) or sorted LT-HSCs (competition assay) from CD45.2^{+} WT or Ptch2$^{-/-}$ mice. (h) Results of LimDilAssay 24 wk after treatment. Long-term engraftment was assessed as positive if chimerism was more than 0.3% CD45.2^{+} PB cells including all lineages. (i) PB chimerism (CD45.2^{+}) of Ptch2$^{-/-}$ HSCs versus WT HSCs compared with CD45.1 control BM cells was assessed by flow cytometry at the indicated time points. PB chimerism of CD45.2^{+} cells of both transplantation groups is shown in one graph. (j) BM cells/tibia, WBC, and hemoglobin levels analyzed 5 and 7 d after 5-FU injection (150 mg/kg BW, $n \geq 3$ each genotype, two independent experiments, unpaired Student's t test). (k) Representative dot plots of LK, LKS, and LK^{med}S cells are shown for each genotype 7 d after the first 5-FU injection. (l) Total LK, LKS, and LK^{med}S cells per tibia 7 d after the first 5-FU injection ($n \geq 3$ each genotype, two independent experiments, unpaired Student's t test). (m) Cell cycle staining for WT (gray) and Ptch2$^{-/-}$ (black) BM cells stained with Ki67 7 d after the first 5-FU injection. (n) Percentage of Ki67^{+} cells in the BM of WT and Ptch2$^{-/-}$ mice 7 d after 5-FU injection ($n \geq 3$ each genotype, two independent experiments, unpaired Student's t test). (o) Kaplan-Meier survival curve of WT and Ptch2$^{-/-}$mice treated weekly with 5-FU (150 mg/kg, Log-rank [Mantel-Cox] test; P = 0.011). *, P < 0.05; **, P < 0.01.

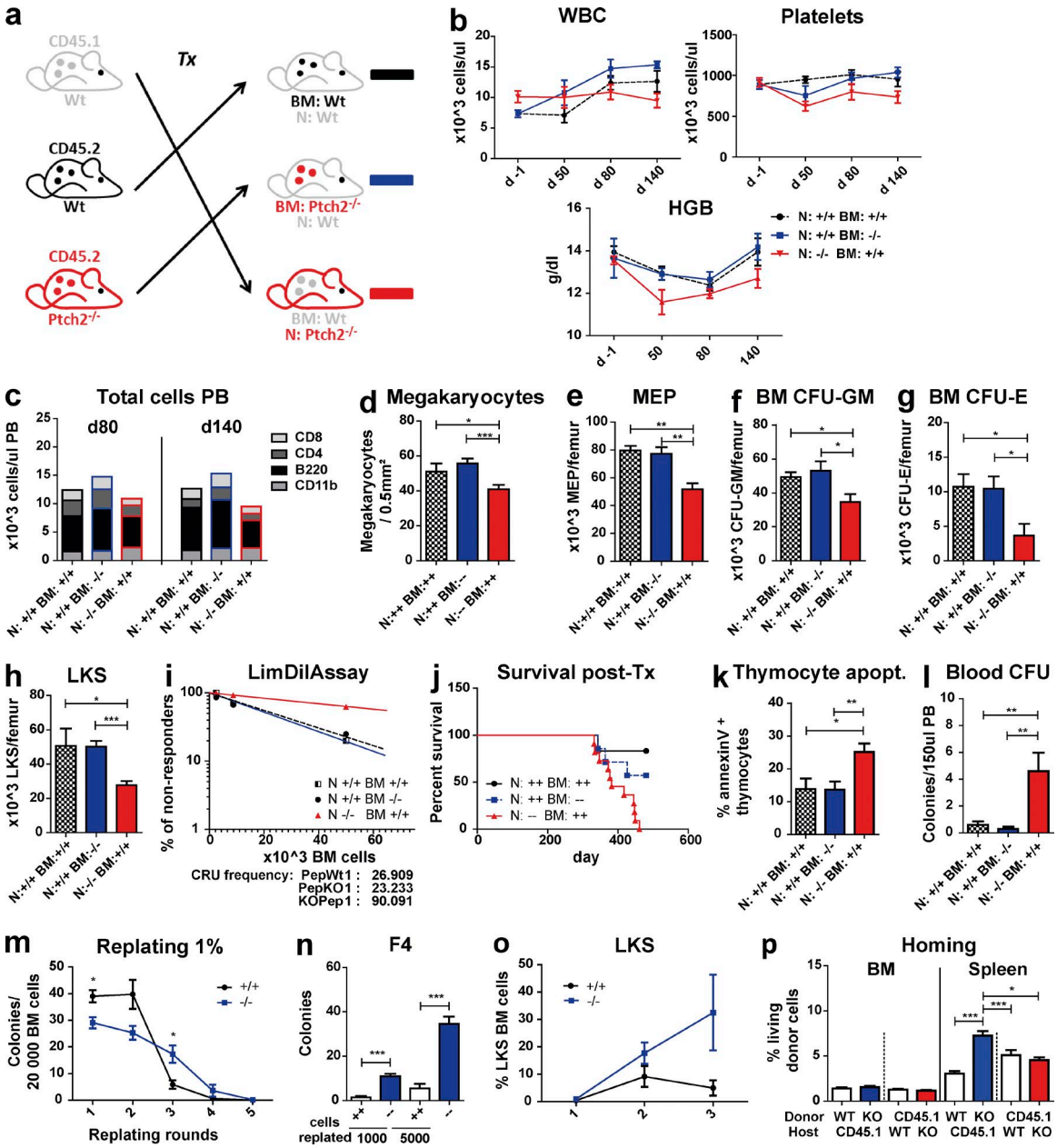

Figure 5. **Niche change experiments reveal counteracting functions of cell-intrinsic and -extrinsic ligand driven HH signaling on hematopoiesis.** (a) Scheme for niche change experiments. Ptch2$^{-/-}$ BM cells (blue; CD45.2$^+$) were transplanted into CD45.1 mice (blue; BM, Ptch2$^{-/-}$; N, WT). WT BM cells (red; CD45.1$^+$) were transplanted into Ptch2$^{-/-}$ mice (CD45.2$^+$; red; BM, WT; N, Ptch2$^{-/-}$) or WT control (black) mice (CD45.2$^+$; black; BM, WT; N, WT). Red, niche Ptch2$^{-/-}$; blue, hematopoietic Ptch2$^{-/-}$. (b) Hemoglobin (HGB) levels, WBC, and platelet counts before and after the niche change at indicated time points ($n \geq 8$ each group, unpaired Student's t test). (c) Total PB cells were subdivided into CD4$^+$ T cells (CD3$^+$CD90$^+$CD4$^+$), CD8$^+$ T cells (CD3$^+$CD90$^+$CD8$^+$), B cells (B220$^+$), and myeloid cells (CD11b$^+$) at day 70 and 140 using flow cytometry ($n \geq 8$ each group, unpaired Student's t test). (d) Megakaryocyte count per 0.5 mm^2 BM slide ($n \geq 4$ each group; unpaired Student's t test). (e) Percentage of MEPs assessed by flow cytometry 4 mo after transplantation ($n \geq 4$ each group). (f) CFU-GM within 20,000 BM cells seeded in MethoCult 3434 and counted 7 d after seeding (4 mo after transplantation, $n \geq 3$ each group, performed in duplicates, unpaired Student's t test). (g) CFU-E within 20,000 BM cells seeded in MethoCult 3434 and counted 7 d after seeding (4 mo after transplantation; $n \geq 3$ each group, performed in duplicates, unpaired Student's t test). (h) Percentage of LKS cells assessed by flow cytometry 4 mo after transplantation ($n \geq 4$ each group, unpaired Student's t test). (i) For LimDilAssays 2.5, 8.75, or 50 × 10^3 BM cells (4 mo after transplantation) were pooled with 10^6 supporting BM cells and transplanted into lethally irradiated CD45.1/45.2 expressing mice. Long-term engraftment and CRU frequency was assessed 24 wk after transplantation (chimerism > 0.3% CD45.2$^+$ PB cells including all lineages. (j) Long-term survival after niche change (Kaplan-Meier curve; k). Total apoptotic (Annexin V$^+$) thymocytes ($n \geq 4$, unpaired Student's t test). (l) CFUs within 150 µl PB seeded in MethoCult 3434 and counted 7 d after seeding ($n \geq 3$ each group, performed in duplicates, unpaired Student's t test). (m) Replating assay of 20,000 WT or Ptch2$^{-/-}$ BM cells plated

mice. To prolong their survival, mice were transplanted with BM containing only 5% BCR-ABL$^+$ cells. In this context, only the cell-intrinsic deletion of Ptch2 enhanced disease development, resulting in an earlier death of the mice by further increasing leukocytosis, whereas the Ptch2$^{-/-}$ niche did not alter disease development (Fig. 7, h and i).

Our findings show that hyperactivation of combined canonical and noncanonical HH signaling in myeloproliferative diseases can accelerate disease development, and in the case of JAK2V617F, can turn a nonlethal myeloproliferative disease into a lethal acute leukemia. Although cell-intrinsic HH activation enhances leukocytosis and splenomegaly in JAK2V617F and BCR-ABL-pos. mice, the niche Ptch2$^{-/-}$ mobilizes leukemic blasts into the PB and enhances thrombocytopenias and anemias, resulting in a premature death of those mice.

DISCUSSION

Aberrant activation of HH signaling in malignancies caused by point mutations in the canonical SMO-dependent HH pathway (PTCH1/SMO mutations) drives specific cancer entities, such as basal cell carcinomas, medulloblastomas, or rhabdomyosarcomas, which in turn are highly responsive to treatment with SMO inhibitors (vismodegib and erismodegib). In contrast, the majority of cancer types show activated HH signaling within the malignant cells or within the surrounding stromal cells induced by excess ligand secretion. Previous clinical trials with SMO inhibitors for these entities have failed to show treatment responses, perhaps because HH ligands stimulate a much broader signaling event, as follows: SMO-dependent canonical GLI1/2 activation; retention of activated CYCLIN B1 in the cytoplasma by binding to PTCH receptors (Barnes et al., 2001); and constitutive ERK activation directly downstream of PTCH1 (Chang et al., 2010). ERK signaling is a major player in the oncogenic RAS signaling pathway cascade, and is involved in driving proliferation, migration, and stemness, through various stages of cancer development. In our experiments, we show that the PTCH1 receptor is the exclusive mediator of ERK signaling induced by HH ligands. The depletion of PTCH1 blocked ERK phosphorylation, whereas depletion of its ligand competitor PTCH2 actually induced ERK phosphorylation, by redirecting the entire ligand toward the PTCH1 receptor. In this regard, Ptch2$^{-/-}$ mice constitute an ideal model to simulate the situation of excess ligand stimulation of effector cells, allowing for the evaluation of its influence on both malignant and niche cells.

Interestingly, in MPNs, but not in AML, we can detect high levels of *DHH* and *PTCH1* in the malignant cells, accounting for activated canonical HH signaling. In addition, we find loss of *PTCH2* in ∼70% of the cases. This is despite the fact that granulocytes and monocytes, which are the main pool of leukocytes within the PB in MPNs, usually have the highest *PTCH2* levels within the whole hematopoietic system (Fig. 1 l). In embryonic development, it was shown that PTCH2 expression is necessary to abrogate canonical HH signals and limits HH activity to the floor plate (Holtz et al., 2013), thus implicating that lack of PTCH2 in myeloid cells/GMPs further amplifies HH ligand stimulatory effects. Indeed, Ptch2$^{-/-}$ mice show massive expansion of granulocytes/monocytes starting at the GMP level, resulting in leukocytosis and splenomegaly, even though the regenerative HSC pool is concomitantly reduced. Interestingly, Dhh$^{-/-}$ mice, which have reduced canonical and noncanonical HH signaling, show the exact opposite phenotype, with a reduction in GMPs and granulocytes, whereas MEPs are increased (Lau et al., 2012). In Ptch2$^{-/-}$ mice, differentiation from CMPs to MEPs is blocked as a result of cell-extrinsic mechanisms. This results in reduced numbers of megakaryocytes and erythroid progenitors in the BM. The effect on erythropoiesis is partially compensated for by the relocation of erythropoiesis into the spleen, further increasing splenomegaly. These myeloproliferative features, with increased granulocytes/monocytes and enhanced erythropoiesis in the spleen and splenomegaly, strongly resemble human MPNs.

In contrast to myeloid cells, Ptch2 is nearly absent in B and T cells, whereas Ptch1 is most strongly expressed. In agreement with these results, hematopoietic Ptch2$^{-/-}$ did not affect B and T cell development, suggesting that the Ptch1 receptor functions as the regulator of cell-intrinsic HH ligand responses in T cell development and T cell activation (Rowbotham et al., 2009; Furmanski et al., 2012; de la Roche et al., 2013). Nevertheless, the niche Ptch2$^{-/-}$ strongly enhances apoptosis rates and reduces the frequencies of all T cell subsets within the thymus, probably as a result of increased selection pressures within the thymic niche.

In addition, lack of Ptch2 in the niche resulted in loss of B cells at 12 mo of age. This is partially caused by the reduction in the HSC pool, which occurs by that time, followed by a reduction in differentiating CLPs. In addition, B cell maturation in the BM is guided by direct interaction of cKit$^+$ pro–B cells with Scf-expressing stromal cells. Because Scf levels are drastically reduced in Ptch2$^{-/-}$ BM niche cells, the development of prepro–B cells is also affected.

in MethoCult3434 and replating of 1% of all cells every 7 d ($n \geq 4$ each genotype, performed in duplicates, unpaired Student's *t* test). (n) Replating assay was started with 20,000 WT or Ptch2$^{-/-}$ BM cells seeded in MethoCult3434. Next, 1,000 or 5,000 BM cells were replated every 7 d. Graph shows colony counts before plating round 4 ($n \geq 3$ each genotype, performed in duplicates). (o) Percentage of LKS cells as assessed by flow cytometry after each replating round ($n \geq 3$ each group). (p) 7×10^6 BM cells were transplanted i.v. into lethally irradiated recipients and spleen homing efficiency was assessed 4 h after treatment by CD45.1/CD45.2 discrimination ($n \geq 5$ each group, unpaired Student's *t* test). *, $P < 0.05$; **, $P < 0.01$; ***, $P < 0.001$.

Table 1. **Findings from the niche change experiment**

Parameters	N: –/–; BM: –/–	N: –/–; BM: +/+	N: +/+; BM: –/–
WBC	++	-	+
Neutrophils	++	+	+
B cells	–	–	+
T cells	–	–	+
HGB	-	-	o
Platelets	-	-	o
LKS	-	–	o
Colonies PB	++	++	o
Homing spleen		o	+
Replating			+

Overview of hematopoietic (right column) or niche (middle column) effects of the Ptch2$^{-/-}$.

The effect of the complete Ptch2$^{-/-}$ LT-HSCs is primarily characterized by an increase in cell cycling, followed by HSC exhaustion after 12 mo, loss of HSC quiescence, and HSC mobilization into the PB and the spleen. Most of the effects on the HSC compartment can be explained by niche cell alterations in Ptch2$^{-/-}$ mice. Cxcl12 is strongly reduced in Ptch2$^{-/-}$ CaR cells. CXCL12 inhibitors are potent HSC mobilizers used in the clinic, and a lack of Cxcl12 reduces HSC retention in the BM, causing HSC mobilization into the PB. Loss of Scf and other self-renewal factors, such as Jagged1, are most likely the cause of the reduction in stem cell maintenance, whereas the loss of megakaryocytes results in strongly increased Thpo levels, driving the cell cycle in HSCs. The influence of the HH signaling pathway on the BM niche is mainly caused by the noncanonical pathway, as Cxcl12-expressing CaR cells, osteoblasts (osteopontin), and endothelial cells only show noncanonical Erk–Ras pathway activation, but not canonical HH pathway activation. The only niche cell type that can activate both the canonical and noncanonical HH signaling pathway is MSPCs. Our findings implicate that excess HH ligand stimulation of the niche cells, or otherwise induced constitutive activation of canonical and noncanonical HH signaling, can strongly alter the production of cytokines important for the maintenance of HSCs, therefore HH ligand–producing malignant cells possess the ability to drastically alter their niche.

Although the Ptch2$^{-/-}$ niche causes loss of HSCs, the intrinsic Ptch2$^{-/-}$ enhances replating capacity and LKS maintenance in vitro. Furthermore, the hematopoietic Ptch2$^{-/-}$ causes leukocytosis by increasing the frequency of nearly all cell types (myeloid cells and B and T lymphocytes). These cell-intrinsic effects are also strongly supported by the experiments using myeloproliferative oncogenes such as BCR-ABL or JAK2V617F. BCR-ABL causes a lethal myeloproliferative disease in mice, and death of the mice was strongly accelerated by hematopoietic Ptch2$^{-/-}$, resulting in faster and more pronounced leukocytosis, whereas cell-extrinsic depletion of Ptch2 was not relevant to disease development. This confirms our previous findings that depletion of hematopoietic canonical HH-signaling (Smo) is relevant for disease development and stem cell function in BCR-ABL–driven disease (Dierks et al., 2008).

The JAK2V617F oncogene causes a myeloproliferative disease in humans, which is stable for years and then progresses to AML in ∼4–12% of the cases. The mechanisms driving this acceleration are currently not understood. In C57BL/6 mice, the JAK2V617F oncogene also causes nonlethal MPN, which is characterized by initial erythrocytosis, followed by leukocytosis and a mild myelofibrosis at later stages. Also in this context, the hematopoietic Ptch2$^{-/-}$ drastically increased leukocytosis, accelerated the infiltration of cells into the spleen, and increased the numbers of Kit^{+} immature blasts in the PB (Fig. 7, b–e). The constitutive activation of canonical and noncanonical HH signaling in niche cells caused mobilization of immature Kit^{+} blasts into the PB, approaching the criteria for a myeloid leukemia, and also increased the severity of anemias and thrombocytopenias, causing death in those mice. These findings are in agreement with previous publications showing that tight control of the niche is necessary to guide HSC maturation and genetic stability, and that loosening this control results in the development of leukemias (Kode et al., 2014).

Finally, the combination of hematopoietic and niche-dependent induction of canonical and noncanonical HH signaling simulates excess HH ligand stimulation in both compartments, transforming the nonlethal myeloproliferative disease into a full-blown acute leukemia, with >30% blasts in the PB and in which all mice succumbed to the disease. These findings suggest that excess HH ligand secretion is also a potential driver of the transformation process of MPNs into acute leukemias in humans. Furthermore, it implicates HH ligand inhibitors instead of SMO inhibitors in fully targeting the canonical and noncanonical HH pathway within hematopoiesis, and the niche as a possible therapeutic option to prevent the transformation of MPNs into acute leukemias.

MATERIALS AND METHODS

Mouse experiments. Ptch1$^{+/-}$ (Ptch1^{tm1Mps}/Ptch1^{+}; The Jackson Laboratory), Ptch2$^{-/-}$ (Ptch2^{tm1Dgen}/Ptch2^{tm1Dgen}; Deltagen), C57BL/6 (Ly5.2), Ly5.1 (B6.SJL-Ptprca Pepcb/BoyJ; The Jackson Laboratory), and Ly5.1/Ly5.2 (Ly5.1 x Ly5.2 crossbreed, both from The Jackson Laboratory) mice were maintained and genotyped as previously described. Ptch1 and Ptch2 mice were backcrossed 10 times with C57BL/6. All mice used for experiments (inclusive control groups) were obtained from our inbred strains. All animal experiments were conducted in compliance with the US Department of Health and Human Service Guide for Care and Use of Laboratory Animals, and in concordance with German law. Experiments were approved by the Regierungspräsidium Freiburg.

For niche change transplantations (Fig. 5 a), BM cells were isolated from donor mice (Ly5.1, Ptch2$^{-/-}$, or C57BL/6) and red blood cells were lysed using Gay solution. 5×10^{6} BM cells were transplanted via retroorbital injection into lethally irradiated (10 Gy) hosts (Ly5.1, Ptch2$^{-/-}$, or C57BL/6). To monitor hematopoietic recovery, blood was analyzed

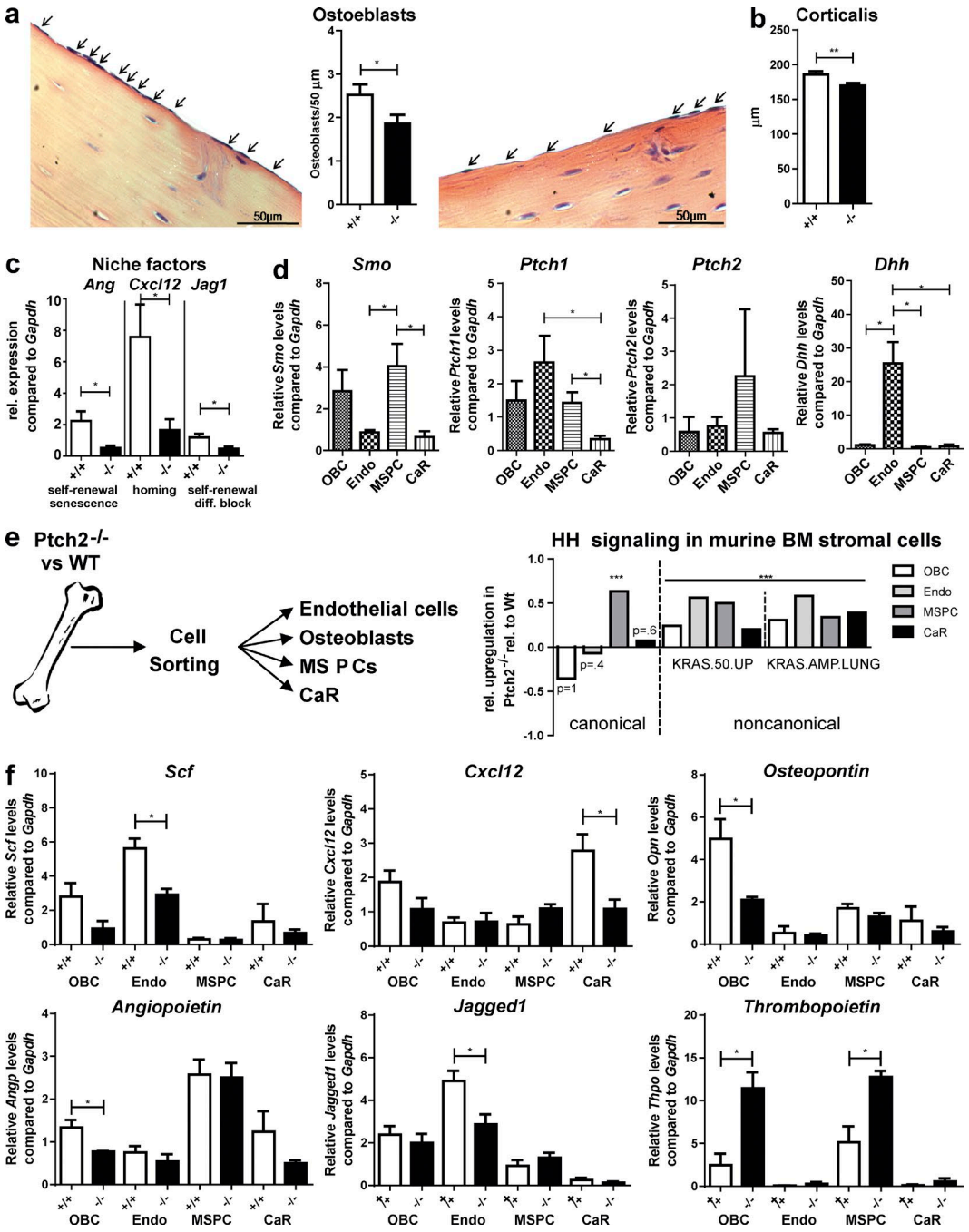

Figure 6. **Ptch2$^{-/-}$ causes depletion of osteoblasts and alters expression of essential HSC retention and maintenance factors within all niche cell subsets.** (a) Representative images from H&E-stained femurs. Arrowheads indicate osteoblasts. Osteoblasts were quantified by counting three images per mouse (n = 6 each genotype, 3 mo, unpaired Student's t test). Bars, 50 µm. (b) Corticalis thickness was measured three times for each sample (n = 10 each genotype, 3 mo, unpaired Student's t test). (c) qPCR for murine *Angiopoietin-1 (Ang)*, *Cxcl12*, and *Jagged1 (Jag1)* in murine BM stroma samples. Transcript levels are shown relative to *Gapdh* and compared with the median of all samples ($n \geq 3$ each genotype, two independent experiments, unpaired Student's t test). (d) qPCR for murine *Smoothened (Smo)*, *Ptch1*, *Ptch2*, and *Desert hedgehog (Dhh)* in sorted osteoblastic (OBC), endothelial (Endo), mesenchymal stem, and progenitor cell (MSPC), and Cxcl12-abundant reticular (CaR) cells. Transcript levels are shown relative to *Gapdh* and compared with the median of all samples (n = 15 each genotype, unpaired Student's t test). (e) RNA samples (n = 15 each genotype) from sorted WT and Ptch2$^{-/-}$ niche cells were analyzed via Affymetrix GeneChip Mouse Gene ST 2.0 and evaluated via KEGG and oncogenic signature gene sets. + indicates significant increased signaling pathways within specified Ptch2$^{-/-}$ subpopulations. (f) qPCR for *Scf*, *Cxcl12*, *Osteopontin (Opn)*, *Angiopoietin-1*, *Jagged1*, and *Thrombopoietin* in sorted osteoblastic (OBC), endothelial (Endo), mesenchymal stem (MSPC), and CaR cells purified from WT and Ptch2$^{-/-}$ mice. Transcript levels are shown relative to *Gapdh* and compared with the median of all samples (n = 15 each genotype, unpaired Student's t test). *, $P < 0.05$; ***, $P < 0.001$.

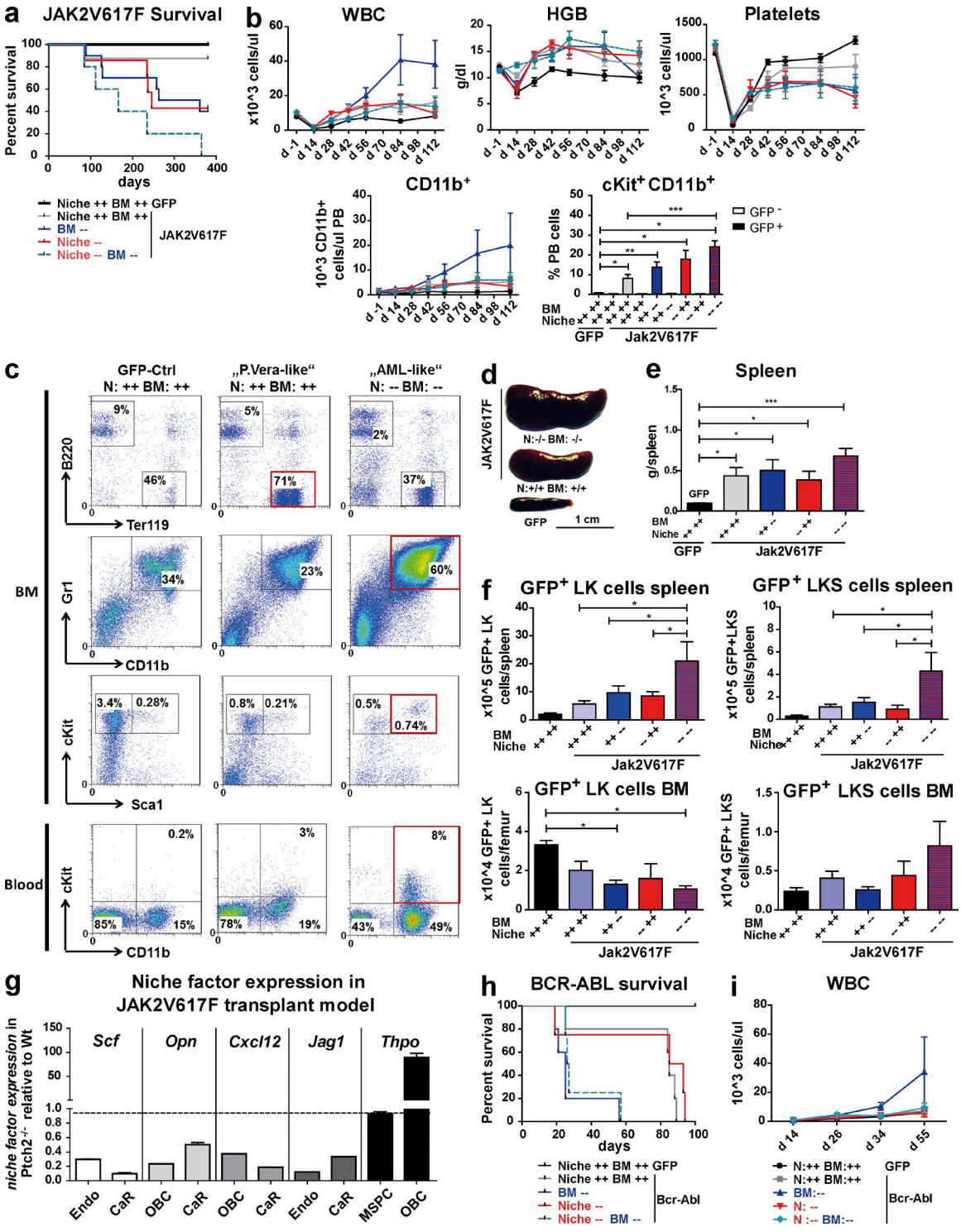

Figure 7. **Cell-intrinsic, but also -extrinsic, Ptch2$^{-/-}$ accelerates myeloproliferative diseases caused by JAK2V617F and converts a chronic polycythemia vera–like disease into a lethal leukemia.** (a) Kaplan-Meier survival curve of WT or Ptch2$^{-/-}$ mice transplanted with JAK2V617F-GFP transduced WT or Ptch2$^{-/-}$ BM cells ($n \geq 5$ each group). (b) PB samples were analyzed for WBC, hemoglobin (HGB), and platelet counts using the Scil Animal Blood Counter. Myeloid PB cells (CD11b$^+$) and cKit$^+$CD11b$^+$ myeloid blasts (d112) were measured by flow cytometry ($n \geq 5$ each group). (c) Representative dot plots of lymphoid B220$^+$, erythroid Ter119$^+$ and myeloid CD11b$^+$GR1$^+$ cells within BM and GFP$^+$cKit$^+$CD11b$^+$ cells (blasts) within PB. (d) Representative image of splenomegaly in JAK2V617F$^+$ Ptch2$^{-/-}$ mice versus JAK2V617F$^+$ WT and GFP control mice. (e). Spleen weight at time of death ($n \geq 5$ each group, unpaired Student's *t* test). (f) GFP$^+$LK and GFP$^+$LKS cells within spleen and BM ($n \geq 5$ each group) at time of death. (g) Expression levels of essential niche

using an ADVIA120 (Siemens). Donor cell engraftment was determined using Ly5.1/Ly5.2 discrimination. For the limiting dilution competitive transplantation assay, we transplanted 1×10^6 Ly5.1 BM with 3×10^3, 15×10^3, 3×10^4, and 1×10^6 competitor Ptch2$^{-/-}$ or C57BL/6 BM cells in lethally irradiated Ly5.1/Ly5.2 recipient mice (Fig. 4 g). For the competitive LT-HSC repopulation assay, 1×10^6 Ly5.1 BM cells were mixed with 150 SLAM$^+$ competitive Ptch2$^{-/-}$ or WT LT-HSCs and transplanted into lethally irradiated Ly5.1/Ly5.2 mice. Engraftment was monitored by Ly5.1/Ly5.2 staining at 4, 8, 12, and 16 wk after transplantation. Engraftment was assessed as positive if chimerism was >0.3% including all lineages.

JAK2V617F and BCR-ABL. For BM transplantation experiments, including retroviral JAK2V617F or BCR-ABL insertion, donor mice (Ptch2$^{-/-}$ or C57BL/6) were injected i.p. with 5-FU (150 mg/kg) and mice were sacrificed 4 d later. RBC-depleted BM cells were cultivated in DMEM containing 10% fetal bovine serum, IL-3, IL-6, and SCF. Cells were infected twice with a pMSCV/JAK2V617F/IRES-GFP or MSCV/BCR-ABL/IRES-GFP or pMSCV/IRES-GFP (control) retrovirus. 5×10^5 mononuclear cells were transplanted retroorbitally into lethally irradiated Ptch2$^{-/-}$ or C57BL/6 mice. Disease development was monitored by inspection for general disease symptoms, twice weekly weight measurements, and blood cell counts (Advia120; Siemens), followed by flow cytometric analysis. BM was aspirated after 100 d, and then analyzed by FACS. Mice were sacrificed when moribund organs of interest (spleen, femur, and liver) were extracted for weight measurements, flow cytometry analysis, or fixed for IHC staining.

Homing assay. 7×10^6 Ly5.1, WT, or Ptch2$^{-/-}$ BM cells were injected i.v. into lethally irradiated Ly5.1, WT, or Ptch2$^{-/-}$ recipient mice. After 4 h, the mice were sacrificed and BM and spleen cells were analyzed using CD45.1/CD45.2 and LIVE/DEAD Fixable Aqua Dead Cell stain (Thermo Fisher Scientific).

Flow cytometry analysis. Antibodies used are as follows (all from BioLegend): CD3, CD11b, Gr1, CD19, Ter119, Il7R (lineage markers), CD31, CD45, CD45.1, CD45.2, CD51, CD4, CD8, B220, CD34, FLT3, CD48, CD150, CD41, CD44, CD16/32, CD90.1 (Thy1.1), CD140 (VEGFR), CD166 (Alcam), cKit, Sca1, and Ki67. For cell cycle analysis, cells were fixed with 2% formalin, permeabilized with chilled 90% methanol, and stained with FxCycle Violet stain (Invitrogen), Ki67, or with Click-iT reagent to detect incorporated BrdU according to the manufacturer's instructions (Invitrogen). BrdU (100 µl/20 g body weight, 10 mM EdU) was injected i.p. 15 h before BM harvest. For intracellular phospho-Erk staining, cells were fixed and permeabilized, and then incubated with a phospho-p42/44 MAPK mouse mAb (Cell Signaling Technology), followed by the secondary anti–mouse IgG Alexa Fluor 488–conjugated Ab (Cell Signaling Technology). Cells were analyzed using a CyanADP flow cytometer. Annexin V/7AAD staining (BD) was performed according to the manufacturer's instructions.

Immunoblotting. Protein expression of PTCH1, PTCH2, ERK, and pERK was determined in 293T cells transfected with siRNA against *PTCH1* or *PTCH2* using standardized protocols with antibodies against the following proteins: PTCH1 (LS-Bio; LS-B3939; 1:1,000), PTCH2 (LS-Bio; LS-C80730; 1:1,000), ERK (Cell Signaling Technology; MAPK, Erk1/2, 9102; 1:1,000), pERK (Cell Signaling Technology; Phospho-p44/42 MAPK, Erk1/2, 9106; 1:1,000), and β-actin (Sigma-Aldrich; 1:20,000).

Immunohistochemistry staining. Paraffin-embedded spleen and liver sections, as well as paraffin-embedded and decalcified BM slides, were acquired from the Pathology Department of the University of Freiburg. Diaminobencidine immunoperoxidase staining (EnVision+System-HRP/DAB; DAKO) was performed for 10 min according to the manufacturer's instructions. Primary Abs to CD11b (IgG rabbit polyclonal; LSBio) diluted 1:400 were incubated overnight, followed by a 30-min incubation with secondary Abs (EnVision+System-HRP/DAB; DAKO). Immunodetection was performed with 3,3 diaminobencidine. HE stain was done for 30–45 s. Images were taken using an Axioplan2 microscope (Carl Zeiss).

BM cultures. Femurs of WT or Ptch2$^{-/-}$ mice were flushed and cells were when cultivated in Petri dishes for 12 d without the addition of cytokines. Floating cells were removed after 24 h, and then every second day, and only adherent cells were used for further analysis regarding HH gene expression, Erk phosphorylation, and the expression of cytokines.

Colony assays. RBC-depleted BM (2×10^4), spleen (5×10^5), and PB cells (5×10^5) were plated in MethoCult GF M3434 (StemCell Technologies, Inc.) and colonies were counted after 7 d. Benzidine staining was performed to identify erythroid colonies.

qPCR. RNA from human PBMCs from patient samples, enriched adherent BM cells, or sorted BM cells was isolated

factors are shown from Ptch2$^{-/-}$ mice (relative to *Gapdh*) compared with WT mice (relative to *Gapdh*), both carrying the JAK2V617F oncogene. Expression levels within WT was set to one (unpaired Student's *t* test). (h) Kaplan-Meier survival curve of WT or Ptch2$^{-/-}$ mice transplanted with BCR-ABL–GFP transduced WT or Ptch2$^{-/-}$ BM cells ($n \geq 4$ each group). (i) PB samples were analyzed for WBC using the Scil Animal Blood Counter ($n \geq 4$ each group). *, $P < 0.05$; **, $P < 0.01$; ***, $P < 0.001$.

using the RNeasyKit (QIAGEN), reverse transcribed, and amplified for 50 cycles at an annealing temperature of 60°C. Murine and human primer/probe sets for TaqMan PCR were obtained from Applied Biosystems (Table S3). Results were quantified according to the ΔΔ-CT method, based on the relative expression of a target gene versus a reference gene (GAPDH), and normalized to the median of all samples.

Gene array. WT and Ptch2$^{-/-}$ niche cells were pooled from five mice and sorted as described in Fig. S1. RNA was extracted with the RNeasy Micro Kit (QIAGEN). RNA integrity was analyzed by capillary electrophoresis using a Fragment Analyzer (Advanced Analytical Technologies). RNA samples had an RNA quality number of >8.5 and were further processed with the NuGEN Ovation Pico WTA V2 Kit as described by the manufacturer. The amplified cDNA was further fragmented and labeled using the Affymetrix WT Terminal labeling and control kit. Labeled fragments were hybridized to GeneChip Mouse Gene ST 2.0 arrays for 16 h at 45°C with 60 rpm in an Affymetrix Hybridization oven 640. After washing and staining, the arrays were scanned with the Affymetrix GeneChip Scanner 3000 7 G. CEL files were produced from the raw data with Affymetrix GeneChip Command Console Software Version 4.0. We used Partek Genomics Suite software for further analysis.

Here, CEL files were imported, including control and interrogating probes. Prebackground adjustment was set to adjust for GC Content and probe sequence and RMA background correction was performed. Arrays were normalized using Quantile normalization, and probeset summarization was done using Median Polish. Probe values were $\log_2$ transformed. To identify differentially expressed genes between the groups, we performed a one-way analysis of variance in Partek. Using Fisher's Least Significant Difference as a contrast method, WT subpopulations (MSPCs, endothelial cells, OBCs, and CaR cells) were compared with Ptch2$^{-/-}$ subpopulations. Gene set enrichment analysis was performed by using the KEGG gene set database or the oncogenic signature gene set database. The threshold for significance was set to a nominal value of $P < 0.05$, normalized enrichment score >1.2 or <−1.2 and false discovery rate <0.25.

Statistical analysis. Data are represented as the mean ± SEM. For statistical comparisons between groups, two-tailed Student *t* test or Mann-Whitney test was performed when indicated. For all analyses, $P < 0.05$ was considered statistically significant: *, $P < 0.05$; **, $P < 0.01$; ***, $P < 0.001$. Correlations were assessed with the Spearman rank correlation coefficient. Analyses were performed using GraphPad Prism 5.03.

Gene accession number. Gene expression data are available from ArrayExpress (accession no. E-MTAB-3361).

Online supplemental material. Fig. S1 shows gating strategies for PB, spleen/BM cells analysis, and niche cell purification. Fig. S2 shows flow cytometry analysis for B cell lymphopoiesis. Fig. S3 shows enrichment plots and heat maps for core enrichment genes. Table S1 lists patient characteristics. Table S2 lists Molecular Signature Database oncogenic signatures. Table S3 lists genes and primers. Online supplemental material is available at http://www.jem.org/cgi/content/full/jem.20150556/DC1.

ACKNOWLEDGMENTS

This work was supported by the Emmy-Noether program of the DFG (DI 1664/1-1), FOR 2033 TP B1 (Nichem), and the Deutsche Krebshilfe (grant 110670). C. Dierks is supported by EXC 294, Centre for Biological Signaling Studies *BIOSS*.

The authors declare no competing financial interests.

Author contributions: C. Klein, A. Zwick, K. Aumann, S. Decker, T. Benkler, and S. Kissel performed the experiments. D. Pfeifer performed Affymetrix arrays. M. Follo performed the cell sorting. A.L. Illert, C. Klein, R.A.J. Oostendorp, C. Dierks, and J. Duyster designed research. C. Klein and C. Dierks wrote the manuscript.

Submitted: 25 March 2015
Accepted: 21 December 2015

REFERENCES

Alfaro, A.C., B. Roberts, L. Kwong, M.F. Bijlsma, and H. Roelink. 2014. Ptch2 mediates the Shh response in Ptch1$^{-/-}$ cells. *Development.* 141:3331–3339. http://dx.doi.org/10.1242/dev.110056

Barnes, E.A., M. Kong, V. Ollendorff, and D.J. Donoghue. 2001. Patched1 interacts with cyclin B1 to regulate cell cycle progression. *EMBO J.* 20:2214–2223. http://dx.doi.org/10.1093/emboj/20.9.2214

Bhardwaj, G., B. Murdoch, D. Wu, D.P. Baker, K.P. Williams, K. Chadwick, L.E. Ling, F.N. Karanu, and M. Bhatia. 2001. Sonic hedgehog induces the proliferation of primitive human hematopoietic cells via BMP regulation. *Nat. Immunol.* 2:172–180. http://dx.doi.org/10.1038/84282

Byrd, N., S. Becker, P. Maye, R. Narasimhaiah, B. St-Jacques, X. Zhang, J. McMahon, A. McMahon, and L. Grabel. 2002. Hedgehog is required for murine yolk sac angiogenesis. *Development.* 129:361–372.

Campaner, S., A. Viale, S. De Fazio, M. Doni, F. De Franco, L. D'Artista, D. Sardella, P.G. Pelicci, and B. Amati. 2013. A non-redundant function of cyclin E1 in hematopoietic stem cells. *Cell Cycle.* 12:3663–3672. http://dx.doi.org/10.4161/cc.26584

Chan, I.S., C.D. Guy, Y. Chen, J. Lu, M. Swiderska-Syn, G.A. Michelotti, G. Karaca, G. Xie, L. Krüger, W.K. Syn, et al. 2012. Paracrine Hedgehog signaling drives metabolic changes in hepatocellular carcinoma. *Cancer Res.* 72:6344–6350. http://dx.doi.org/10.1158/0008-5472.CAN-12-1068

Chang, H., Q. Li, R.C. Moraes, M.T. Lewis, and P.A. Hamel. 2010. Activation of Erk by sonic hedgehog independent of canonical hedgehog signalling. *Int. J. Biochem. Cell Biol.* 42:1462–1471. http://dx.doi.org/10.1016/j.biocel.2010.04.016

Datta, S., and M.W. Datta. 2006. Sonic Hedgehog signaling in advanced prostate cancer. *Cell. Mol. Life Sci.* 63:435–448. http://dx.doi.org/10.1007/s00018-005-5389-4

Decker, S., K. Zirlik, L. Djebatchie, D. Hartmann, G. Ihorst, A. Schmitt-Graeff, D. Herchenbach, H. Jumaa, M. Warmuth, H. Veelken, and C. Dierks. 2012. Trisomy 12 and elevated GLI1 and PTCH1 transcript levels are biomarkers for Hedgehog-inhibitor responsiveness in CLL. *Blood.* 119:997–1007. http://dx.doi.org/10.1182/blood-2011-06-359075

de la Roche, M., A.T. Ritter, K.L. Angus, C. Dinsmore, C.H. Earnshaw, J.F. Reiter, and G.M. Griffiths. 2013. Hedgehog signaling controls T cell killing at the immunological synapse. *Science.* 342:1247–1250. http://dx.doi.org/10.1126/science.1244689

Dierks, C., J. Grbic, K. Zirlik, R. Beigi, N.P. Englund, G.R. Guo, H. Veelken, M. Engelhardt, R. Mertelsmann, J.F. Kelleher, et al. 2007. Essential role of stromally induced hedgehog signaling in B-cell malignancies. *Nat. Med.* 13:944–951. http://dx.doi.org/10.1038/nm1614

Dierks, C., R. Beigi, G.R. Guo, K. Zirlik, M.R. Stegert, P. Manley, C. Trussell, A. Schmitt-Graeff, K. Landwerlin, H. Veelken, and M. Warmuth. 2008. Expansion of Bcr-Abl-positive leukemic stem cells is dependent on Hedgehog pathway activation. *Cancer Cell.* 14:238–249. http://dx.doi.org/10.1016/j.ccr.2008.08.003

Dyer, M.A., S.M. Farrington, D. Mohn, J.R. Munday, and M.H. Baron. 2001. Indian hedgehog activates hematopoiesis and vasculogenesis and can respecify prospective neurectodermal cell fate in the mouse embryo. *Development.* 128:1717–1730.

Furmanski, A.L., J.I. Saldana, N.J. Rowbotham, S.E. Ross, and T. Crompton. 2012. Role of Hedgehog signalling at the transition from double-positive to single-positive thymocyte. *Eur. J. Immunol.* 42:489–499. http://dx.doi.org/10.1002/eji.201141758

Gao, J., S. Graves, U. Koch, S. Liu, V. Jankovic, S. Buonamici, A. El Andaloussi, S.D. Nimer, B.L. Kee, R. Taichman, et al. 2009. Hedgehog signaling is dispensable for adult hematopoietic stem cell function. *Cell Stem Cell.* 4:548–558. http://dx.doi.org/10.1016/j.stem.2009.03.015

Gering, M., and R. Patient. 2005. Hedgehog signaling is required for adult blood stem cell formation in zebrafish embryos. *Dev. Cell.* 8:389–400. http://dx.doi.org/10.1016/j.devcel.2005.01.010

Goodrich, L.V., and M.P. Scott. 1998. Hedgehog and patched in neural development and disease. *Neuron.* 21:1243–1257. http://dx.doi.org/10.1016/S0896-6273(00)80645-5

Gorlin, R.J. 1987. Nevoid basal-cell carcinoma syndrome. *Medicine.* 66:98–113. http://dx.doi.org/10.1097/00005792-198703000-00002

Greenbaum, A., Y.M. Hsu, R.B. Day, L.G. Schuettpelz, M.J. Christopher, J.N. Borgerding, T. Nagasawa, and D.C. Link. 2013. CXCL12 in early mesenchymal progenitors is required for haematopoietic stem-cell maintenance. *Nature.* 495:227–230. http://dx.doi.org/10.1038/nature11926

Hofmann, I., E.H. Stover, D.E. Cullen, J. Mao, K.J. Morgan, B.H. Lee, M.G. Kharas, P.G. Miller, M.G. Cornejo, R. Okabe, et al. 2009. Hedgehog signaling is dispensable for adult murine hematopoietic stem cell function and hematopoiesis. *Cell Stem Cell.* 4:559–567. http://dx.doi.org/10.1016/j.stem.2009.03.016

Holtz, A.M., K.A. Peterson, Y. Nishi, S. Morin, J.Y. Song, F. Charron, A.P. McMahon, and B.L. Allen. 2013. Essential role for ligand-dependent feedback antagonism of vertebrate hedgehog signaling by PTCH1, PTCH2 and HHIP1 during neural patterning. *Development.* 140:3423–3434. http://dx.doi.org/10.1242/dev.095083

Kawamura, S., K. Hervold, F.A. Ramirez-Weber, and T.B. Kornberg. 2008. Two patched protein subtypes and a conserved domain of group I proteins that regulates turnover. *J. Biol. Chem.* 283:30964–30969. http://dx.doi.org/10.1074/jbc.M806242200

Kobune, M., Y. Ito, Y. Kawano, K. Sasaki, H. Uchida, K. Nakamura, H. Dehari, H. Chiba, R. Takimoto, T. Matsunaga, et al. 2004. Indian hedgehog gene transfer augments hematopoietic support of human stromal cells including NOD/SCID-$\beta 2m^{-/-}$ repopulating cells. *Blood.* 104:1002–1009. http://dx.doi.org/10.1182/blood-2003-09-3347

Kode, A., J.S. Manavalan, I. Mosialou, G. Bhagat, C.V. Rathinam, N. Luo, H. Khiabanian, A. Lee, V.V. Murty, R. Friedman, et al. 2014. Leukaemogenesis induced by an activating β-catenin mutation in osteoblasts. *Nature.* 506:240–244. http://dx.doi.org/10.1038/nature12883

Lau, C.I., S.V. Outram, J.I. Saldaña, A.L. Furmanski, J.T. Dessens, and T. Crompton. 2012. Regulation of murine normal and stress-induced erythropoiesis by Desert Hedgehog. *Blood.* 119:4741–4751. http://dx.doi.org/10.1182/blood-2011-10-387266

Lunardi, S., R.J. Muschel, and T.B. Brunner. 2014. The stromal compartments in pancreatic cancer: are there any therapeutic targets? *Cancer Lett.* 343:147–155. http://dx.doi.org/10.1016/j.canlet.2013.09.039

Maye, P., S. Becker, H. Siemen, J. Thorne, N. Byrd, J. Carpentino, and L. Grabel. 2004. Hedgehog signaling is required for the differentiation of ES cells into neurectoderm. *Dev. Biol.* 265:276–290. http://dx.doi.org/10.1016/j.ydbio.2003.09.027

Mendelson, A., and P.S. Frenette. 2014. Hematopoietic stem cell niche maintenance during homeostasis and regeneration. *Nat. Med.* 20:833–846. http://dx.doi.org/10.1038/nm.3647

Merchant, A., G. Joseph, Q. Wang, S. Brennan, and W. Matsui. 2010. Gli1 regulates the proliferation and differentiation of HSCs and myeloid progenitors. *Blood.* 115:2391–2396. http://dx.doi.org/10.1182/blood-2009-09-241703

Motoyama, J., T. Takabatake, K. Takeshima, and C. Hui. 1998. Ptch2, a second mouse Patched gene is co-expressed with Sonic hedgehog. *Nat. Genet.* 18:104–106. http://dx.doi.org/10.1038/ng0298-104

Perry, J.M., O.F. Harandi, P. Porayette, S. Hegde, A.K. Kannan, and R.F. Paulson. 2009. Maintenance of the BMP4-dependent stress erythropoiesis pathway in the murine spleen requires hedgehog signaling. *Blood.* 113:911–918. http://dx.doi.org/10.1182/blood-2008-03-147892

Poulos, M.G., P. Guo, N.M. Kofler, S. Pinho, M.C. Gutkin, A. Tikhonova, I. Aifantis, P.S. Frenette, J. Kitajewski, S. Rafii, and J.M. Butler. 2013. Endothelial Jagged-1 is necessary for homeostatic and regenerative hematopoiesis. *Cell Reports.* 4:1022–1034. http://dx.doi.org/10.1016/j.celrep.2013.07.048

Rowbotham, N.J., A.L. Hager-Theodorides, A.L. Furmanski, S.E. Ross, S.V. Outram, J.T. Dessens, and T. Crompton. 2009. Sonic hedgehog negatively regulates pre-TCR-induced differentiation by a Gli2-dependent mechanism. *Blood.* 113:5144–5156. http://dx.doi.org/10.1182/blood-2008-10-185751

Siggins, S.L., N.Y. Nguyen, M.P. McCormack, S. Vasudevan, R. Villani, S.M. Jane, B.J. Wainwright, and D.J. Curtis. 2009. The Hedgehog receptor Patched1 regulates myeloid and lymphoid progenitors by distinct cell-extrinsic mechanisms. *Blood.* 114:995–1004. http://dx.doi.org/10.1182/blood-2009-03-208330

Sugiyama, T., H. Kohara, M. Noda, and T. Nagasawa. 2006. Maintenance of the hematopoietic stem cell pool by CXCL12-CXCR4 chemokine signaling in bone marrow stromal cell niches. *Immunity.* 25:977–988. http://dx.doi.org/10.1016/j.immuni.2006.10.016

Thayer, S.P., M.P. di Magliano, P.W. Heiser, C.M. Nielsen, D.J. Roberts, G.Y. Lauwers, Y.P. Qi, S. Gysin, C. Fernández-del Castillo, V. Yajnik, et al. 2003. Hedgehog is an early and late mediator of pancreatic cancer tumorigenesis. *Nature.* 425:851–856. http://dx.doi.org/10.1038/nature02009

Uhmann, A., K. Dittmann, F. Nitzki, R. Dressel, M. Koleva, A. Frommhold, A. Zibat, C. Binder, I. Adham, M. Nitsche, et al. 2007. The Hedgehog receptor Patched controls lymphoid lineage commitment. *Blood.* 110:1814–1823. http://dx.doi.org/10.1182/blood-2007-02-075648

Watkins, D.N., D.M. Berman, S.G. Burkholder, B. Wang, P.A. Beachy, and S.B. Baylin. 2003. Hedgehog signalling within airway epithelial progenitors and in small-cell lung cancer. *Nature.* 422:313–317. http://dx.doi.org/10.1038/nature01493

Zhao, C., A. Chen, C.H. Jamieson, M. Fereshteh, A. Abrahamsson, J. Blum, H.Y. Kwon, J. Kim, J.P. Chute, D. Rizzieri, et al. 2009. Hedgehog signalling is essential for maintenance of cancer stem cells in myeloid leukaemia. *Nature.* 458:776–779. http://dx.doi.org/10.1038/nature07737